EUROPEAN ORGANIZATION FOR NUCLEAR RESEARCH

CERN-PPE/91-107
24 June 1991

# On Muon Production and other Leakage Aspects of Pion Absorption in a Lead/Scintillating-Fiber Calorimeter

D. Acosta[1)], S. Buontempo[2)], L. Calôba[3)], M.Caria[4)], R. DeSalvo[5a)], A. Ereditato[2)], R. Ferrari[6)], G. Fumagalli[6)], G. Goggi[5,6)], W. Hao[5b)]†, F.G. Hartjes[7)], A. Henriques[5,8)], L. Linssen[5a)], M. Livan[4)], A. Maio[8)], L. Mapelli[5)], M.R. Mondardini[9)], B. Ong[1)], H.P. Paar[1)], F. Pastore[6)], E. Pennacchio[6)], L. Poggioli[10)], G. Polesello[5,6)], F. Riccardi[2)], A. Rimoldi[6)], C.V. Scheel[5a,7)], J. Schmitz[7)], J.M. Seixas[3,5)], A. Simon[11)], M. Sivertz[1)], P. Sonderegger[5)], M.N. Souza[3)], Z.D. Thomé[3)], V. Vercesi[6)], Y. Wang[5b)]†, R. Wigmans[5,7)], C. Xu[5b)]† and K. You[5b)]†

1) *University of California, San Diego, USA*
2) *Università di Napoli and INFN Sez. Napoli, Italy*
3) *COPPE/EE/UFRJ, Rio de Janeiro, Brazil*
4) *Università di Cagliari and INFN Sez. Cagliari, Italy*
5) *CERN, Geneva, Switzerland*
5a) *CERN/LAA project, Geneva, Switzerland*
5b) *CERN (Worldlab fellowship), Geneva, Switzerland*
6) *Università di Pavia and INFN Sez. Pavia, Italy*
7) *NIKHEF-H, Amsterdam, the Netherlands*
8) *LIP, Lisbon, Portugal*
9) *Cornell University, Ithaca, USA*
10) *LPNHE, Université Paris VI&VII, Paris, France*
11) *Universität Heidelberg, Heidelberg, Germany*

† On leave of absence from IHEP Beijing, China

**Abstract**

We report on an experimental study of longitudinal leakage phenomena in hadronic shower development. Pions in the energy range of 10 - 150 GeV were sent into a lead/scintillating-fiber calorimeter with a thickness of 9.5 nuclear interaction lengths. The average fraction of the energy leaking out at the back of this calorimeter ranges from 0.04% at 10 GeV to 0.4% at 150 GeV. This leakage has a very small effect on the hadronic energy resolution. We measured the probability of the creation of escaping muons in the shower development process. This probability ranges from 0.2% at 10 GeV to 2.1% at 150 GeV. Assuming that these muons are produced from $\pi$- or $K$-decay, we find an exponentially decaying muon spectrum with a typical momentum of 2.8 GeV/c, at 80 GeV incident energy. Also the rates at which hadrons and soft neutrons escape from the calorimeter are measured. Within the acceptance of the leakage calorimeter, neutrons are observed about 10 times as often as muons. Escaping hadrons dominate muons for shower energies above 20 GeV. The experiments were performed at CERN in the framework of the LAA project.

(Submitted to Nuclear Instruments and Methods in Physics Research)

## 1. INTRODUCTION

The new generation of multi-TeV high-luminosity $pp$ colliders (LHC, SSC) is an enormous challenge for detector development. The detectors in experiments at these machines will have to be able to handle event rates up to (and maybe larger than) 1 GHz, to extract the interesting physics at trigger levels of $10^{-8}$ and below, and to survive a considerable radiation load.

Crucial in any of these experiments will be the calorimeter system. Apart from its role in providing the first-level trigger information and in detecting the production of jets, electrons and neutrinos (missing energy), the calorimeter serves as a muon filter. One of the important questions that needs to be answered when designing an experiment concerns the thickness of the calorimeter. The choice of this parameter will have repercussions for:

- The quality of the calorimeter information itself. Increased shower leakage will for example deteriorate the energy resolution.
- The muon detectors. Shower leakage will cause hits in these detectors, which will make it more difficult to trigger on the particles for which they are designed (e.g. muons from the process $H \rightarrow ZZ \rightarrow \mu\mu\mu\mu$).
- The cost of the experiment, which for many components scales as $r^2 - r^3$, $r$ being the distance to the interaction point. For example, the instrumented volume of a calorimeter with an effective nuclear interaction length ($\lambda_I$) of 20 cm, starting at 1 m from the vertex, increases by a factor 1.5 when its thickness is increased from $10\lambda_I$ to $12\lambda_I$. And the volume of a muon detector covering $\Delta r = 2$ m increases by a similar factor when a $10\lambda_I$ deep calorimeter with $\lambda_I = 30$ cm is used instead of $\lambda_I = 20$ cm (both starting at $r = 1$ m).

The Spaghetti Calorimeter was developed, in the framework of the LAA project at CERN, as a dedicated calorimeter for LHC/SSC experiments. It is an (almost) compensating lead/scintillating-fiber calorimeter with monolythic towers, i.e. without longitudinal segmentation into an electromagnetic (e.m.) and an hadronic section. Among its many remarkable properties, which are described elsewhere[1-6], we mention one that is particularly relevant in view of what was said before, namely its very compact construction. Because of the large fraction of high-$Z$ absorber material (78% in volume, sampling fraction for showers only 2.3%), needed in order to achieve compensation[7], the effective radiation length ($X_0$) amounts to 7.2 mm, the effective Molière radius ($R_M$) to 20 mm, the effective nuclear interaction length[8] $\lambda_I$ to 21 cm and the average density to 9.0 g/cm$^3$. These numbers are almost the same as for the ZEUS calorimeter[9], which contains the much denser $^{238}$U as absorber material.

In this paper, we report on the results of an experimental study of longitudinal shower leakage effects for pion absorption in the 200 cm (9.5 $\lambda_I$) deep Spaghetti Calorimeter. Since the shower leakage was measured with a fine-grained calorimeter as well, we were able to distinguish between several types of shower leakage. Most frequently, the signals in the leakage detector were caused by escaping neutrons. Charged particle leakage from showers caused by pions that undergo their first interaction very deep inside the main calorimeter (*punch-thru*) was observed as well, especially at the highest energies.

A particularly interesting category of leakage events are the ones in which a muon is generated in the hadronic shower development. This phenomenon, which is mainly caused by secondary and higher order pions and kaons that decay before they (strongly) interact, is of course important for the muon detectors located downstream in an experiment. We were able to identify such muons, determine their probability of being created in hadronic showers and measure their energy spectrum. Also the rates at which other types of particles escape the calorimeter were measured.

In section 2, the detectors used for these studies, their calibration and the experimental setup are described. Section 3 deals with the experimental data and with the event selection. Section 4 gives results on the shower leakage as a function of energy and angle, and on the effects of leakage on the calorimeter performance. In section 5, the signal from muons generated in the hadronic shower development is analyzed, and the rates at which muons, hadrons and soft neutrons escape the detector are determined. A summary and conclusions are presented in section 6.

## *2. EXPERIMENTAL SETUP*

### 2.1 The detector

The measurements were performed with 2 calorimeters consisting of longitudinally unsegmented towers. Each tower contains 1141 plastic scintillating fibers* each with a diameter of 1 mm and a length of 2.20 m. These fibers form the active part of the sampling calorimeters. They are embedded in a lead matrix in such a way that each fiber is equidistant to its 6 neighbors (fig. 1a). The fiber spacing is 2.22 mm (center to center), such as to achieve a volume ratio lead:fiber of about 4:1, needed in order to make the calorimeter (approximately) compensating[7,10] .

* SCSF-38, produced by Kyowa Gas, now Kuraray Co. Ltd, Tokyo, Japan

The fibers were grouped to form towers. Each tower has an hexagonal cross section (86 mm apex to apex). The depth of the lead structure is 200 cm. The fibers sticking out at one end of the tower were bunched together in an hexagonal structure, machined and polished and coupled through an hexagonal light guide (79 mm long, 42 mm apex to apex) to a photomultiplier (PM)** . The other end of each fiber was polished and made reflective by aluminium sputtering, such as to make the response more uniform as a function of the position along the fiber. More detailed information about the structure of the calorimeters is given in ref. 2.

The main calorimeter, to be called SPACAL in the following, consists of 155 towers. A central tower is surrounded by 7 concentric hexagonal rings (see fig. 1b); with the outer ring incomplete, the detector has roughly a cylindrical shape with a diameter of 1 meter. In the tests described in this paper, this detector was installed as intended in experiments for which it was developed, namely with the fibers running in (almost) the same direction as the beam particles and the readout located at the back end of the detector. Therefore, its dimensions amounted to 9.5 $\lambda_I$ in depth and 4.8 $\lambda_I$ across.

The second detector, to be called LC (Leakage Calorimeter) in the following, has the same structure but is smaller. It consists of 20 hexagonal towers with exactly the same characteristics as the towers in the big detector. They were grouped as indicated in fig. 1c: A central tower surrounded by 2 hexagonal rings plus one extra tower further outside. This detector served as a leakage calorimeter in the tests described here. It was installed behind the SPACAL detector, with the fibers running *perpendicular* to the beam. In this way, the leakage calorimeter provided an extra 30-35 cm ($1.5 - 1.7\ \lambda_I$) of *longitudinally subdivided* calorimetry. It covered 35% of the back plane of the SPACAL detector and stuck out laterally by 50 cm on each side (see fig. 2).

The PM signals were handled as follows. The anode signal from each SPACAL tower was split into 2 equal parts by means of a passive splitter inside the base. One part went to the counting room where it was further fed into an active splitter, one output of which was sent unchanged into a 12-bit charge ADC, the other output was amplified by a factor $\sim 10$ before being fed into an ADC. The other half of the anode signal went into a linear adder, where it was combined with tower signals from the same hexagonal ring. The resulting ring sum signals were treated in the same way as the signals that were directly sent to the counting room. The signals of the leakage calorimeter were only split at the ADC level, but not inside the PM base.

** Philips XP 2282, 8-stage

The gain in the PM tubes was set to deliver $\sim$ 4 pC/GeV in the central detector region, gradually going up to $\sim$ 20 pC/GeV in the outer rings of the SPACAL detector, for the unamplified channels. For the channels of the leakage calorimeter, the gain was $\sim$ 10 pC/GeV for particles hitting it in the middle (because of light attenuation in the fibers, the signal is position dependent in this geometry). The ADC gain was 4 counts/pC. This procedure was chosen to circumvent the insufficient dynamic range of our PM/ADC system and to be sensitive to small energy deposits far away from the shower axis.

The data discussed in this paper were taken at an ADC gate width of 400 ns. Sparse data readout was enabled: signals smaller than 4 counts above the pedestal value were not recorded. This corresponds to a cutoff of 5 MeV energy deposits in the amplified channels of the outer SPACAL rings and of 10 MeV for the amplified channels of the leakage detector.

### 2.2 The beam line

The measurements were performed in the H2 beam line of the SPS at CERN. The SPACAL detector was mounted on a platform that could move horizontally and vertically with respect to the beam line, with a precision of about 1 mm. Moreover, the detector could be rotated around its vertical axis, so that the particles could be sent into the detector at a chosen angle $\theta_z$ (usually a few degrees) with respect to the fiber axis. The precision of the angular movement was better than 0.1 mr. On the other hand, the actual value of the angle was only known to within $\sim 1/2^0$. In the following, the mentioned values of $\theta_z$ are nominal ones. There are indications that the real angles between the particle direction and the fiber axis were about $1/2^0$ smaller than the nominal ones (see sect. 4.2).

The leakage calorimeter was installed on a fixed platform behind the SPACAL detector as described in sect. 2.1. The distance between the sensitive volumes of SPACAL and the leakage calorimeter amounted to 80 cm. The beam line passed $\sim$ 3 cm below the geometrical center of the leakage calorimeter.

About 12 cm upstream of the SPACAL calorimeter, a preshower detector was mounted. This preshower detector (PSD) consisted of an absorber sheet (1.14 $X_0$ tungsten + 0.53 $X_0$ lead), followed by a scintillation counter (S6). The signal in this scintillator provided a clean (at energies above 40 GeV about a factor 10) separation between electron and pion events[3] . Further upstream of the calorimeters, a trigger counter telescope was installed. It consisted of 5 scintillation counters (S1 - S5) and 2 drift chambers with $x$,$y$ readout (BC1, BC2). The layout is shown in fig. 2.

Beams of negative pions of 5, 10, 20, 40, 80 and 150 GeV were sent into the detector at a small angle $\theta_z$ with respect to the fiber axis. The beam particle rates were $10^2 - 10^3$ events per spill. The spills lasted for 2.6 s and were repeated every 14 s. At high energies ($\geq$ 40 GeV) the beams were very clean, the contamination of electrons in the pion beam being below the 1% level. At lower energies this was different. The contaminating electrons could be efficiently removed with the help of the PSD data. At 5 and 10 GeV, where the beams were heavily contaminated, the PSD signal was part of the trigger. For pions, the S6 signal was required to be below a threshold, set at $\sim 7$ times the minimimum ionizing value. Since the PSD covered only an area of $15 \times 15$ cm$^2$ in the central region of the calorimeter, it was removed during scans in which a larger SPACAL area was investigated.

The pion beams also contained some fraction of muons, which were very important for the present analysis. This fraction varied from $\sim$ 2% at 150 GeV to $\sim$ 80% at 5 GeV. The $\pi/\mu$ separation will be described in detail in the sections 3 and 5.

Off-line event selection required a single track, by cutting on the pulse height of the scintillation counters S1,2,3 between 0.5 and 1.7 times the minimum ionizing particle (mip) value. The S6 signal was required to be smaller than 2 mip. The $x$ and $y$ coordinates measured in the two beam chambers had to agree within 1 cm. Beam halo particles were removed by cuts on $x$ and $y$ in the beam chambers.

### 2.3 Calibration of the detectors

The SPACAL calorimeter was calibrated with 40 GeV electrons. About 1500 electrons were sent into the central region of each of the 155 individual towers, at an angle $\theta_z$ of $3^0$ to the fiber axis. In this way, on average $\sim$ 95% of the electromagnetic shower energy was deposited in the tower concerned. Off-line, the calibration constants (the relation between picocoulombs and GeV's for each individual tower) could be determined with a statistical precision of $\sim$ 0.3% from this data. Because of systematic effects, due to fiber-to-fiber response fluctuations, high-voltage instabilities, etc. the tower-to-tower calibration is much less precisely known, to about 3%[6] .

For the leakage calorimeter, the calibration procedure was different. First, the gain factors of the 20 individual towers were equalized using muons contaminating the 5 GeV pion beam. Because of the large width of this muon beam and because of multiple scattering in the $266X_0$ of lead preceding the leakage detector, each tower was traversed by a sufficiently large number of particles, ranging from $\sim$ 800 in the 10 towers close to the beam line down to $\sim$ 100 for the towers located farthest away from this line (see fig. 1c). The 5 GeV muons lost a

substantial fraction of their energy (on average about half) when traversing the $9.5\lambda_I$ deep SPACAL detector and, therefore, the muons used to calibrate the leakage calorimeter carried typically only $2-3$ GeV. Figure 3a shows the signal distribution for these muons traversing one of the towers (no. 11, see fig. 1c) of the leakage calorimeter. The energy deposit is very small, typically $\sim 80$ MeV, which is 3 orders of magnitude less than the energy of the particles normally used for calibration purposes. The distribution of the total leakage calorimeter signal from these muons is shown in fig. 3b. The statistical precision of the calibration constants obtained in this way ranged from $\sim 2\%$ in the central region (near the beam line) of the leakage calorimeter to $\sim 6\%$ in the towers located farthest away from the beam line.

After equalizing the gains, the overall scale factor was determined from a run in which a broad beam of 40 GeV electrons was sent directly into the leakage detector, with the SPACAL calorimeter moved out of the way. The fact that the 40 GeV electron signals, the sum of largely fluctuating contributions from several towers, were reconstructed with a reasonable energy resolution ($\sim 6\%$, versus 3.5% for electrons contained in one tower, the method used for calibrating SPACAL) illustrates that this calibration method, based on particles that deposited on average only 80 MeV in the detector cells, worked in principle well enough for our purpose.

## *3. EXPERIMENTAL DATA AND METHODS*

The results described in the following sections were obtained by analyzing the following sets of data:

- Pions of 10, 20, 40, 80 and 150 GeV entering the SPACAL calorimeter at an angle $\theta_z = 0^0$ or $3^0$ to the fiber axis. Typically, $\sim$ 5000 events were accumulated per run. Similar data at 5 GeV were not used for this analysis because of the large contamination by muons and electrons and because of the resulting difficulty of creating a sufficiently large and clean sample of pion events.
  As shown in the previous section, the contaminating 5 GeV muons were used to calibrate the leakage calorimeter.
- Pions of 40 GeV entering the SPACAL detector at angles $\theta_z$ ranging from $0^0$ to $5^0$, in steps of $1^0$. Also here, $\sim$ 5000 events were recorded at each angle.
- A large statistics run for 80 GeV pions at $\theta_z = 2^0$, entering the SPACAL detector at different impact points, in contrast to the other mentioned data,

where the pions always hit the SPACAL detector in the center. Another difference with the other data sets was the absence of the preshower detector. In total, $\sim 10^5$ events were accumulated.

In order to produce clean pion samples, the contaminating electron and muon events had to be removed. This was easiest at the highest energies ($\geq$ 40 GeV), where the beams were very clean to start with, and where the contaminating particles produced very different signals in the various detectors. The few electrons were efficiently removed on the basis of the signal in the preshower detector (see sect. 2.1). The muons were removed with a cut on the total energy deposited in the SPACAL calorimeter. The muon signal in SPACAL was well-described by a Landau distribution with a most probable value of 4-5 GeV, depending on the muon energy and could, therefore, be very easily distinguished from the high-energy pion signals. This is illustrated in fig. 4, which shows a scatter plot of the signals for 80 GeV particles. The signal in the leakage detector is shown versus the signal in the main calorimeter. Clearly, a cut on the signal in the latter is a very efficient means of separating pions from muons. Figure 4 also shows that all muons produce a non-zero signal in the leakage calorimeter, clustering around 400 MeV (see also fig. 3b), while a large majority of the pions are fully contained in the SPACAL detector (zero in the leakage calorimeter). However, since the analysis of the signals from the leakage calorimeter is the subject of this study, these signals could obviously not be used for defining a clean sample of pions.

The complete elimination of muons from the event samples became gradually more difficult at lower energies, where the pion signals in SPACAL were correspondingly smaller. The signals from the muons remained essentially the same and the fraction of muons increased sharply. Therefore, an additional criterion was developed, based on the energy deposit pattern in the SPACAL calorimeter. The criterion exploits the fact that muons, which predominantly lose their energy through ionization, only produce signals in a very limited number of towers, contrary to showering pions. This is illustrated in fig. 5, where the fraction ($f_3$) of the total signal recorded in the 3 SPACAL towers that gave the largest contribution to it is plotted against the total signal in the SPACAL calorimeter, for the particles from the 10 GeV beam. It can be seen that, for example, a cut $f_3 < 95\%$ removes practically all the muons, while almost all pions pass such a cut. Using this criterion, it was possible to define very clean pion event samples, also at low energies. Even at 5 GeV, where pions and muons produce on average almost the same signal in the SPACAL calorimeter, the particles could be efficiently separated through cuts exploiting the differences in the energy deposit pattern.

The numbers of pion events that were used for the present analysis are listed

in Tables 1a and 1b, for $\theta_z = 0^0$ and $3^0$, respectively. The numbers of pions at 5 GeV were considered too small for a meaningful analysis. The numbers of 40 GeV pion events from the angular scan are given in Table 2.

## *4. EXPERIMENTAL RESULTS ON SHOWER LEAKAGE*

In this section, we present results of the analysis of the signals observed in the leakage calorimeter for the samples of pions that were obtained as described in sect. 3. We concentrate on the following issues:

- The fraction of the energy leaking out as a function of the energy of the incident pion.
- The fraction of the energy leaking out as a function of the angle of incidence of the showering pion.
- The effect of longitudinal shower leakage on the energy resolution for pion detection in the SPACAL calorimeter.

In this analysis, we only study longitudinal leakage phenomena. Side leakage from the detector, which has a diameter of $4.8\lambda_I$, was analyzed in another paper[6] and was found to range from $1.5\% - 2.6\%$ in the energy range considered. Before describing the results in detail, we have to address one aspect that is important for all the results obtained from the leakage calorimeter data, namely the fact that this calorimeter had a limited geometrical acceptance.

### 4.1 Acceptance effects on the leakage results

As is shown in fig. 2, the leakage calorimeter covered only $\sim$ 35% of the back plane of the main calorimeter. In the horizontal plane, full coverage was achieved, but vertically only an area ranging from -14 cm to +20 cm around the beam axis was covered by the leakage detector, which corresponds to an opening angle of 120 mr with respect to the SPACAL calorimeter front face. Therefore, some fraction of the particles leaking out at the back of the calorimeter should have missed the leakage detector.

In order to estimate this fraction, the vertical profile of the shower leakage was analyzed. Only the pion events giving a signal larger than 25 MeV in the leakage calorimeter were used for this purpose. For these events, the average energy deposited in each of the 20 cells of the leakage calorimeter was calculated. Figure 6a shows the distribution of these averages as a function of the vertical position of the centers of these cells, for 80 GeV pions incident at $\theta_z = 2^0$. From a Gaussian fit to this data, we estimated that 25% of the leakage energy escaped the leakage calorimeter in this case.

A second reason why the energy measured with the leakage calorimeter is an underestimate for the leakage is the limited depth of this detector, $\sim 1.7\lambda_I$. In order to estimate the leakage beyond the leakage detector, the same data from fig. 6a were used. In fig. 6b, the average measured leakage energy per cell is given as a function of the depth of the cell center, again for 80 GeV pions incident at $\theta_z = 2^0$. From an exponential fit to this data, we estimated that 26% of the leakage energy penetrated beyond the leakage calorimeter at this energy. The total acceptance of the leakage calorimeter was, therefore, $0.75 \times 0.74 = 0.55$.

The description of the lateral and longitudinal profiles in the leakage calorimeter with a Gaussian and an exponential function, respectively, is based on assumptions that are not necessarily valid. Therefore, the calculated acceptance has rather large uncertainties. Also, the acceptance measurement requires considerable statistics in order to be precise. Since the fraction of the events that produced any signal at all in the leakage calorimeter was very small, adequate statistics were only available for the 80 GeV pion run at $\theta_z = 2^0$, where $\sim 10^5$ events were accumulated. Attempts to determine the acceptance for other beam energies gave results that were within the experimental uncertainties equal to the one mentioned before, but these uncertainties were rather large, typically $\sim 10\%$. We therefore decided to use the same acceptance (55%) throughout the analysis and added a systematic error of 10% to all our results, implying that we do not claim to know the fraction of the leakage energy that goes undetected by the leakage calorimeter with a relative precision better than $20 - 25\%$.

### 4.2 The average energy leakage from pion showers

On average, the fraction of the shower energy contained in the 9.5 $\lambda_I$ deep SPACAL calorimeter was large. In Tables 1a,b the fraction of pion events that deposited no measurable energy (defined as $E_{LC} < 25$ MeV) in the leakage calorimeter is listed for the different pion energies. The fraction of fully contained events ranged from 98% at 10 GeV to 75% at 150 GeV, for the data taken at $\theta_z = 3^0$. For the $0^0$ runs, the leakage was slightly larger. When the cutoff value was raised to $E_{LC} = 125$ MeV, as was done for the analysis in our other papers, the fraction of contained events increased to $> 99\%$ at 10 GeV and to 86% at 150 GeV. The value of 125 MeV was chosen, since it is the minimum amount of energy that can be deposited by a muon traversing the leakage calorimeter (see fig. 3b) and, therefore, such a cut automatically removes all muon contamination. The energy dependence of the shower leakage is given in fig. 7. The figure shows for which fraction of the events the energy measured in the leakage calorimeter exceeds a certain percentage of the shower energy. Results are given as a function of this percentage for pions at different energies. From this figure, one sees for

example that the fraction of the events that are contained to better than 99% ranges from 99.5% at 20 GeV to 94% at 150 GeV.

A typical spectrum for the energy deposited in the leakage calorimeter for the case in which the events were not fully contained is given in fig. 8. This energy spectrum, for 80 GeV pions at $\theta_z = 2^0$, is roughly exponential, with a mean value $< E_{LC} > \approx 0.4$ GeV. As may be expected, $< E_{LC} >$ is strongly correlated with the energy of the incoming pion. From the fraction of fully contained events, from $< E_{LC} >$ and from the acceptance of the leakage calorimeter, the average energy leakage per incoming pion $\bar{E}_{LC}$ was calculated. The results are given in Tables 1a,b. In fig. 9, the leakage is given as a fraction of the energy of the incoming pion, as a function of the pion energy. The leakage fraction ranges from 0.04% at 10 GeV to 0.40% at 150 GeV, for $\theta_z = 3^0$. For $\theta_z = 0^0$ the numbers are slightly larger. One may wonder where this difference between the $0^0$ and $3^0$ data comes from. Of course, when the particles enter the SPACAL detector at an angle, the calorimeter becomes effectively deeper and, therefore, the showers will be better contained. However, the difference in effective depth between these two angles amounts only to $2000[1/\cos(3^0) - 1] = 2.7$ mm, or $0.013\lambda_I$, which should not produce any significant effect at all.

In order to understand this difference between the two angles of incidence, the data taken for 40 GeV pions at a whole range of angles $\theta_z$ was analyzed in the same way. The results are given in Table 2. Figure 10 shows the fraction of the energy leaking out at the back of the SPACAL calorimeter as a function of the angle of incidence $\theta_z$. The leakage is approximately constant, except for very small angles. This can be understood as follows. At very small angles, the pions entering the calorimeter at a fiber position may travel quite a long distance inside this fiber. Since the nuclear interaction length of polystyrene is much longer than for the calorimeter as a whole (80 cm versus 21 cm), such pions will penetrate deeper inside the calorimeter before starting a shower and, therefore, the effective depth of the calorimeter is reduced. Actually, the largest leakage signals were observed for $\theta_z = 1^0$ instead of $0^0$. This may be an indication that what was believed to be the $0^0$ detector position corresponded in reality to $\theta_z \sim -1/2^0$, which is possible given the precision of the detector alignment (see sect. 2.2).

### 4.3 Effects of leakage on the calorimeter performance

In order to study the effects of shower leakage on the performance of the SPACAL calorimeter, we compared the signal distributions in this detector for the event samples without any measurable leakage ($E_{LC} < 25$ MeV) to the distributions for the unbiased event samples. The results are given in fig. 11. Figure 11a shows the effect on the energy resolution if only contained showers are

considered (see Table 1b for the fraction of these events). The energy resolution improves a little bit, especially of course at the highest energies where the leakage is largest. Up to $\sim$ 40 GeV, the improvement is barely significant, but at 150 GeV there is a 9% effect. When one looks at $\sigma_{RMS}$ instead of the $\sigma$ derived from the Gaussian fit, the effects are larger. This may be understood from the fact that leakage events produce a relatively large fraction of their light close to the PM's, where the fiber's light attenuation curve rises steeply. The signal distribution for those events is therefore more non-Gaussian than the distribution for the contained events[6] .
We also studied the effect on the energy resolution for the events with $E_{LC} <$ 125 MeV, our standard cut for other types of data analysis. As expected, the effects are smaller, since fewer events are rejected in this way. The improvement in the energy resolution for 150 GeV pions (by far the worst case) as a result of this containment cut amounts to 7%, for the Gaussian fit.

The effect of containment cuts on the average signal observed in the SPACAL calorimeter is smaller than 1.5% in all cases. Figure 11b shows that the average signal *decreases* if only contained pion showers are taken into account. At first sight this may seem strange, since one would expect an effect with the opposite sign. This phenomenon is due to the peculiarities caused by light attenuation in the fibers.

Pions interacting deep inside the SPACAL detector will produce larger signals than those interacting early on, since the scintillation light is less attenuated. And since such deeply penetrating pions are also more likely to cause a signal in the leakage calorimeter, a positive correlation between the amplitudes of the signals in the leakage calorimeter and the SPACAL calorimeter may be expected. We checked this in the following way. Knowing the impact point of the particles from the beam chamber data (fig. 2), one can infer the effective depth of the shower ($< z >$) from the lateral displacement ($\Delta x$) of the center of gravity of the shower with respect to this impact point, since $\Delta x =< z > \sin(\theta_z)$[4] . In fig. 12, the average signal in the SPACAL calorimeter and the average fraction leaking out at the back of this detector are given as a function of $< z >$, confirming that on average both the signal and the leakage increase if the shower develops deeper inside the calorimeter. Selecting contained events will therefore tend to reduce the calorimeter signal. The reduction amounted to at maximum 0.8% or 1.2%, at 150 GeV, depending on whether the average signal was calculated on the basis of the Gaussian fit or from the actual signal distribution. These numbers changed to 0.6% and 0.9%, respectively, when the leakage cutoff was increased to $E_{LC} = 125$ MeV.

Therefore, we conclude that the effects of shower leakage on the calorimeter

performance (fig. 11) are marginal for a detector of this thickness, even at the highest energies at which it was tested.

## *5. THE PARTICLES ESCAPING FROM THE CALORIMETER*

In this section, we determine which types of particles escape the calorimeter and at which rates. In the last part of the section, hadrons and soft neutrons are discussed, but first we will describe the results of a study of muon production in hadronic shower development. Such muons may for example be produced when secondary, tertiary or higher-order pions or kaons decay before (strongly) interacting. This phenomenon may be highly disturbing in physics experiments. It was presumably mainly responsible for the like-sign dimuon signals observed in high energy $\nu$ and $\bar{\nu}$ scattering[11] .

Evidence for the production of muons in hadronic shower development can be seen from fig. 13. In this figure, the energy spectrum measured in the leakage calorimeter for 80 GeV pions at $\theta_z = 2^0$ (fig. 13a) is compared with the spectrum that beam muons produce in this detector (fig. 13b). The bump observed around $\sim 0.4$ GeV is most probably due to muons produced in the shower development process.

### 5.1 The rates of muon production

In order to determine the rate of muon production in hadronic shower development, the detailed event information provided by the fine-grained detector system was fully exploited. All candidate events were examined individually in order to see whether or not they had the very characteristic signature of the phenomenon looked for. From the muon contamination in the pion beams, it was found that these particles deposit typically 400 MeV in the leakage detector, and that the probability of producing signals smaller than 100 MeV or larger than 1.5 GeV is negligibly small (see fig. 3b). Also, when looking at the signals in the individual towers in the leakage calorimeter, a very characteristic track pattern was observed (fig. 14). The probability of the energy deposit in one individual tower exceeding 0.3 GeV is negligibly small (see fig. 3a). Therefore, events of the type shown in fig. 15 could be ruled out as muon candidates. The most likely explanation for events of this type is that a charged hadron escaped from the SPACAL calorimeter, penetrated the leakage calorimeter and interacted in it, producing several other particles, most of them nuclear fragments with a very short range, hence the large signal in the tower in which this happened. Of course, by ruling out such events as muon candidates, we neglect the possibility that a muon is accompanied by one or several hadrons escaping the calorimeter. How-

ever, this probability was calculated to be small compared to the experimental errors, except possibly at 150 GeV.

Most frequently, events producing a signal in the leakage calorimeter exhibited a pattern as shown in fig. 16. Only one or a small number of towers at random positions inside the leakage calorimeter were fired. Especially the events in which small signals in the leakage detector were observed, smaller than the 0.4 GeV typical for a minimum ionizing particle traversing this detector, were of this type. Such events are most likely caused by neutrons escaping from the back of the SPACAL calorimeter and scattering off a proton in the plastic fibers of the leakage calorimeter. The densely ionizing recoil protons from this process have a range that is typically much shorter than the fiber cross section and, therefore, relatively large signals can be expected.

Especially at low energies, much care had to be taken in order not to confuse muons produced in the hadronic shower development with contaminating muons from the beam. Although cuts on the total energy deposited in the SPACAL detector removed the overwhelming majority of the beam muons (see fig. 4) even a very small fraction of the beam muons passing such cuts (e.g. events from the Landau tail!) could substantially affect the results because of the small probability of muon production in the hadronic shower development.

In order to avoid this problem, the energy deposit profiles in the leakage calorimeter and in SPACAL were examined in conjunction with one another. As was shown in fig. 5, the energy deposit profiles of muons and pions in the SPACAL calorimeter differ substantially, providing a very efficient means of distinguishing muons produced in the hadronic shower development from beam contamination. This is illustrated in fig. 17, which shows the energy deposit profiles in the SPACAL and leakage detectors for a typical pion event in which a muon is produced (fig. 17a) and for a beam muon that produced such a large signal in SPACAL that it passed the cuts (fig. 17b). Both events occurred in the 40 GeV beam. The beam muon could be easily recognized since it deposited energy almost exclusively in one tower of the SPACAL calorimeter, which is very unlikely to happen in case of a pion shower (see fig. 5).

From scanning all the events that produced a sufficiently large signal in the leakage calorimeter, we found that most of the muon candidates in the 10 and 20 GeV beams were of the type shown in fig. 17b and, therefore, were caused by the Landau tail of the beam contaminating muons. Even at 40 GeV, a few events of this type were found. All events producing a signal between 0.1 and 1.5 GeV in the leakage detector were individually examined. In order to be considered a muon candidate, the event had to exhibit a track pattern in the leakage detector of the type shown in fig. 17, with none of the individual towers

exceeding 0.3 GeV. Events for which more than 95% of the energy deposited in SPACAL was concentrated in 3 (or fewer) towers were discarded as being beam contaminating muons. The resulting numbers of muons generated in the hadronic shower development are given in Table 3, for $\theta_z = 0^0$. The uncertainty margins given in this table are the statistical errors, added in quadrature with the uncertainty arising from a few boundary cases and with the uncertainty on the calorimeter acceptance. In this case, the acceptance correction only had to account for muons that passed under or over the leakage calorimeter (lateral acceptance). We used the standard factor of 0.75 (see sect. 4.1) for this purpose. The table also lists the probability that a muon is produced in the hadronic shower development. This probability is given as a function of the pion energy in fig. 18, showing proportionality within experimental errors. A least squares fit to the experimental data yields as the probability for the generation of muons that carry sufficient energy to escape the SPACAL calorimeter and produce a track in the leakage calorimeter

$$P_\mu = 1.3 \times 10^{-4} E$$

per shower, with the pion energy $E$ given in GeV.

Muon production in hadronic shower development is presumably mainly due to shower particles (mainly $\pi$ and $K$) that decay in flight. Since the number of different shower particles susceptible to decay is to first order proportional to the energy of the incoming pion, this result is not surprising. In second order, deviations from proportionality might be expected due to the energy-dependent e.m. shower component (leading to reduced $\mu$-production at higher energy) and to threshold effects (associated production, charmed particles), which work in the opposite direction. Detailed Monte Carlo simulations will be needed to understand the magnitude and the energy dependence of the observed phenomena.

### 5.2 The muon energy spectrum

In the previous subsection, we demonstrated that pion showers are a source of muons escaping the SPACAL calorimeter at a rate of $\sim 1.3 \times 10^{-4} E$/shower. In this subsection, we try to determine the momentum of these muons, which is of course another important input parameter for designing a muon spectrometer behind a calorimeter in a realistic experiment. Since our experimental setup did not contain such a spectrometer, we had to rely, also for this purpose, exclusively on calorimetric data. As a consequence, the muon momentum could not be measured directly, but only through the *missing energy*, from a comparison of the SPACAL signals for showers with and without a muon. This missing energy concerns, therefore, the energy of the particle that produced the muon at the

moment of its decay minus the energy that the muon deposited in SPACAL on its way out. For the most likely processes, $\pi \rightarrow \mu\nu$ and $K \rightarrow \mu\nu$, we will thus measure $E_{miss} = E_\mu + E_\nu$, where $E_\mu$ is the energy of the escaping muon. The relation between $E_\mu$ and $E_{miss}$ depends, therefore, among other things on the ratio of decaying $\pi$'s and $K$'s ($E_\mu$ will on average be much closer to $E_{miss}$ for a decaying $\pi$), and requires elaborate Monte Carlo simulations to be established.

From Table 3, one sees that the number of pion showers in which a muon was generated was very small. As a consequence, all that could be determined from this data was the *average* value of the missing energy for the events in which a muon was produced. This quantity was determined as the difference between the average SPACAL signal for contained pion showers and the average SPACAL signal for the sample of events in which a muon was generated. The results are given in the last column of Table 3. At low energies, the numbers of events are so small that $< E_{miss} >$ is not significantly different from 0, but the results obtained at 40, 80 and 150 GeV seem to indicate that $< E_{miss} >$ amounts to $\sim 3-6$ GeV and rises with the pion energy.

More significant information on this topic came from the high statistics run at 80 GeV ($\theta_z = 2^0$). From the initial sample of $\sim 10^5$ events, $\sim 500$ passed cuts that were designed to select events with the appropriate energy deposit profile in the leakage calorimeter. In fig. 19, the signal distribution for this sample of pion showers in which a muon was generated is compared with the signal distribution for contained showers, on a logarithmic scale. The "muon" event distribution exhibits a low-energy tail, which is consistent with an exponentially falling $E_{miss}$ distribution. The Gaussian component common to all SPACAL signal distributions was unfolded by fitting the data from fig. 19b to an expression of the following type:

$$I(E) \;=\; I_0 \int_0^{+\infty} e^{-(E-x)^2/2\sigma^2}\, e^{-x/<E_{miss}>}\, dx$$

where the width $\sigma$ of the Gaussian component was obtained from the contained events (fig. 19a). In this way, it was found that the average value for $E_{miss}$ amounts to $5.2 \pm 0.6$ GeV.

Let us assume that the muons were produced on average at the shower maximum, which was measured to be located on average at a depth of 55 cm inside the calorimeter[4] . The muons have then lost on average 1.5 GeV on their way out of the SPACAL calorimeter. This means that the average energy of the decaying pion or kaon that produced the muon was $5.2 + 1.5 = 6.7$ GeV. If the muon originated from $K$-decay, the accompanying neutrino carried on average 3.2 GeV

away, leaving 2.0 GeV for the escaping muon. If the muon was produced from $\pi$-decay, the neutrino has taken on average 1.5 GeV, so that the escaping muon carried 3.7 GeV. Therefore, we conclude from our data, that the muons produced in the hadronic shower development and escaping the $9.5\lambda_I$ deep SPACAL calorimeter had an average momentum of $2.8 \pm 0.9$ GeV/c.

### 5.3 The punch-thru composition

In sect. 5.1 it was already shown that the energy deposit pattern in the leakage calorimeter could be used to identify the particles that escaped the calorimeter. In particular, it was possible to distinguish between muons, hadrons and soft neutrons (figs. 14-16). We used this information to determine the relative rates of these escaping particles.

All events depositing between 0.1 and 2.5 GeV in the leakage calorimeter (the range in which muons are found) were individually scanned. The criteria for identifying the escaping particle as a muon were already discussed before. The particle was called a neutron if at least 90% of the leakage energy was deposited in one tower (see fig. 16) or in several isolated towers (multiple neutrons). All the other escaping particles were classified as hadrons (probably mainly charged pions). The events depositing more than 2.5 GeV in the leakage calorimeter were also assumed to be caused by escaping hadrons and the events depositing between 25 and 100 MeV (i.e. less than the energy deposited by a minimum ionizing particle traversing the leakage calorimeter) were classified as neutrons. The observed numbers of neutrons, muons and hadrons are listed as a function of the energy of the incoming pion in Table 4.

Figure 20 shows the rates of neutrons and charged hadrons escaping the detector as a function of the shower energy. These rates are normalized to the rate of muon production in hadronic shower development. The data are not corrected for the acceptance of the leakage detector, but this is only a second-order effect in this case, since only *differences* in the acceptance for the different particles will affect the results. We did not have enough experimental information to measure such differences. The figure shows that most of the escaping particles are neutrons. The number of neutrons producing a signal of at least 25 MeV in the leakage calorimeter is about an order of magnitude larger than the number of muons. It should be emphasized that this cutoff value of 25 MeV actually corresponds to neutrons with a kinetic energy of only $\sim$ 0.5 MeV, since these neutrons are *not* sampled like charge particles, but transfer (on average 50% of) their energy in elastic collisions with protons in the scintillator material. The rise of the neutron/$\mu$ ratio at low energy is probably not significant. Pedestal fluctuations beyond the cutoff value of 4 ADC counts (see sect. 2.1) in any one of

the 20 leakage calorimeter towers would cause a similar effect, if such fluctuations were to occur in a few percent of the events. We have some evidence that this is indeed the case.

The rate of pions, kaons and other hadrons escaping the detector increasingly dominates the muon rate at increasing energies. This reflects the fact that the longitudinal shower size increases with energy. While the probability for muon production is to first approximation proportional to the number of shower particles and thus to the shower energy, the *fraction* of the shower particles that escape from the detector can be expected to increase with the shower energy.

We conclude that for a calorimeter of this thickness ($9.5\lambda_I$) the charged particles escaping the detector are predominantly hadrons, except at energies below $\sim$ 20 GeV, where muons become dominating. This conclusion is in qualitative agreement with the results of Fesefeldt and coworkers[12] , who studied the punch-thru phenomena in great detail by means of Monte Carlo simulations. One of their conclusions is that *fast* escaping particles ($p > 25$ GeV/c) are predominantly hadrons up to calorimeter thicknesses of $\sim 18\lambda_I$ (for a shower energy of 300 GeV). A detailed comparison with their predictions is impossible because of the detector specific character of the data.

Nevertheless, the type of information discussed in this paper is likely to be a very sensitive and detailed test for Monte Carlo programs simulating hadronic shower development and, therefore, we have started such simulations for our own detector and experimental circumstances.

## *6. SUMMARY AND CONCLUSIONS*

We have studied longitudinal leakage phenomena in hadronic shower development in a 9.5 nuclear interaction lengths deep lead/scintillating-fiber calorimeter. The particles leaking out at the back of this detector were measured with a $1.7\lambda_I$ deep calorimeter of the same type. The average fraction of the shower energy that escaped detection by the $9.5\lambda_I$ deep calorimeter ranged from 0.04% at 10 GeV to 0.4% at 150 GeV, for pions incident at an angle $\theta_z$ to the fiber axis larger than $1^0$. For smaller angles, an effective reduction of the calorimeter depth, due to particles penetrating deeply in the low-$Z$ active material before interacting, was observed. The effects of longitudinal shower leakage on the hadronic energy resolution and response were very small for this calorimeter. On the other hand, a clear correlation was observed between the signal in the leakage detector and the depth at which the pion started showering in the main calorimeter.

Thanks to the fine-grained nature of the leakage calorimeter, several types of shower leakage could be distinguished. Most frequently, the signals in the

leakage calorimeter were caused by escaping neutrons. The largest signals in the leakage detector were caused by charged hadrons escaping from the back of the calorimeter and causing nuclear interactions in the leakage detector. A particularly interesting category of leakage events are the ones in which a muon was generated in the hadronic shower development. We were able to identify such muons, and determined their probability of being created to range from $\sim 0.2\%$ at 10 GeV to $\sim 2.1\%$ at 150 GeV. From the calorimetric measurement of the missing energy associated with the production of such muons, it was found that the muon energy spectrum is exponentially decreasing. For 80 GeV pions, the mean value of the missing energy was measured to be $5.2 \pm 0.6$ GeV, which translates into an average momentum of 2.0-3.7 GeV/c for the escaping muon, depending on the relative contributions of $K$- and $\pi$-decay as a source of these muons. Within the acceptance of the leakage calorimeter ($\sim 55\%$ averaged over all types of particles), neutrons were observed about 10 times as often as muons. Hadrons dominated muons for shower energies above 20 GeV.

It should be emphasized that the results obtained in this study are specific for this particular calorimeter. The rates of muon production, for example, are likely to be different for other $9.5\lambda_I$ deep calorimeters. We mention two factors that play a role in this:

- The $Z$ of the absorber material determines which fraction of the shower energy is spent on nuclear breakup. In iron calorimeters, on average $\sim 20\%$ of the non-e.m. energy is used for this purpose, versus $\sim 40\%$ in lead structures[7] . And therefore, more pions and kaons (and thus muons) will be produced in hadronic shower development in iron calorimeters than in lead ones.
- The decay probability for pions and kaons produced in the shower development is proportional to the mean free path between nuclear interactions and, therefore, to the effective nuclear interaction length $\lambda_I$ of the calorimeter. A compact construction will limit the muon production rate.

Because of its high-$Z$ absorber material and its extremely compact construction ($\lambda_I \sim 21$ cm), the SPACAL calorimeter is probably one of the best possible options if minimizing the rates of muon production is an experimental design goal. But even so, the data presented in this paper show that, at event rates of 2.7 GHz and 50 GeV hadronic energy dumped in the calorimeters per minimum bias event ($|\eta| < 3$), as in the high-luminosity LHC option[13] , muon rates at the 100 MHz level beyond the calorimeters have to be envisaged.

**Acknowledgements**

We are deeply grateful to the LAA Project Leader, Prof. A. Zichichi, for his vision, his warm interest and his encouraging support. We thank our colleagues from the UA2 Group, and in particular P. Jenni, who helped us in many ways, in particular when running the beam tests. The work described in this paper would have been impossible without the outstanding technical support provided by our technicians O. Barnaba, C. Baudoin, M. Borriello, S. Bricola, J.-M. Chapuis, C. Farella, B. Foligne, A. Freddi, G. Improta, G. Iuvino, F. Pagano, S. Robinson, R. Rocco, L. Rose-Dulcina, G. Sannier, C. Schillinger, A. Sigrist and V. Vanzanella. Financial support from the Istituto Nazionale di Fisica Nucleare to the Cagliari, Napoli and Pavia groups, from the Conselho Nacional de Desenvolvimento Cientifico e Tecnologico of Brazil to the Rio de Janeiro group, and from the U.S. Department of Energy and National Science Foundation to the San Diego group is acknowledged. And finally, we are grateful to the staff of the SPS, and in particular to N. Doble, for the excellent beam conditions and assistance provided during our tests.

# REFERENCES


1. R. DeSalvo *et al.*, Nucl. Instr. and Meth. **A279** (1989) 467.
2. D. Acosta *et al.*, Nucl. Instr. and Meth. **A294** (1990) 193.
3. D. Acosta *et al.*, Nucl. Instr. and Meth. **A302** (1991) 36.
4. D. Acosta *et al.*, Localizing particles showering in a Spaghetti Calorimeter, preprint CERN-PPE/91-11 (1991), to be published in Nucl. Instr. and Meth.
5. D. Acosta *et al.*, Effects of radiation damage on scintillating fibre calorimetry, preprint CERN-PPE/91-45 (1991), submitted to Nucl. Instr. and Meth.
6. D. Acosta *et al.*, Electron, pion and multiparticle detection with a lead/ scintillating-fiber calorimeter, CERN preprint CERN-PPE/91-85 (1991), to be published in Nucl. Instr. and Meth.
7. R. Wigmans, Nucl. Instr. and Meth. **A259** (1987) 389.
8. We define the *nuclear interaction length* $\lambda_I$ in the same way as the Particle Data Group in Phys. Lett. **B239** (1990), page III 5,6. It is the mean free path for *protons* between inelastic interactions. We will use the symbol $\lambda_\pi$ for pions. Since the inelastic cross sections for protons are 50% larger than for pions, $\lambda_\pi \approx 1.5\lambda_I$.
9. U. Behrens *et al.*, Nucl. Instr. and Meth. **A289** (1990) 115.
10. E. Bernardi *et al.*, Nucl. Instr. and Meth. **A262** (1987) 229.
11. H. Burkhardt *et al.*, Z. Phys. **C31** (1986) 39.
12. H. Fesefeldt *et al.*, Nucl. Instr. Meth. **A292** (1990) 279.
13. G. Jarlskog and D. Rein (eds.), Proceedings of the Large Hadron Collider Workshop, Aachen 1990, CERN 90-10, vol. 1.

# FIGURE CAPTIONS

1. Detail of the front face of the calorimeter (a) and the lateral structure of the SPACAL (b) and leakage (c) detectors. The arrows indicate the direction of the particles leaking into the backing calorimeter.
2. Layout of the beam line. See text for details
3. Signal distributions for the muons that were used to calibrate the leakage calorimeter. These muons carried on average an energy of $\sim 3$ GeV. Shown are the signal distributions for one of the towers (no. 11, see fig. 1c) traversed by such muons (a) and for the total leakage calorimeter (b).
4. Scatter plot of the signals in the leakage calorimeter versus the signals in the SPACAL calorimeter, for 80 GeV particles. The pions and muons can be very clearly separated by a cut on the SPACAL signal.
5. The total SPACAL signal versus the fraction $f_3$ of the signal recorded in the 3 *hottest* SPACAL towers, for 10 GeV particles. A cut at $f_3 = 95\%$ yields a very clean separation between pions and muons.
6. Distribution of the average energy per cell in the leakage calorimeter as a function of the vertical cell position (a) and as a function of the thickness of the material upstream (b), for 80 GeV $\pi^-$ at $\theta_z = 2^0$ producing signals larger than 25 MeV in the leakage calorimeter as a whole.
7. The fraction of the events for which more than a certain percentage of the shower energy escapes from the back of the SPACAL detector. Results are given as a function of this percentage, for incoming pions at different energies.
8. Energy spectrum in the leakage calorimeter for pion showers that were not fully contained in the SPACAL calorimeter. Data for 80 GeV $\pi^-$ at $\theta_z = 2^0$.
9. The fraction of energy leaking out at the back of the SPACAL detector, as a function of the energy of the incoming pion. Data taken at $\theta_z = 0^0$ and at $3^0$.
10. The fraction of energy leaking out at the back of the SPACAL calorimeter as a function of the angle $\theta_z$ between the incoming pions and the fiber axis in SPACAL. Data for 40 GeV $\pi^-$.
11. The effects of a containment cut $E_{LC} < 25$ MeV on the energy resolution (a) and the mean signal (b) of the SPACAL calorimeter. Shown are the ratios of the energy resolution or the average signal for the contained events and the energy resolution or the average signal for the unbiased event sample, as a function of the pion energy. Data for $\theta_z = 3^0$.

12. The average signal in the SPACAL calorimeter (a) and the average energy fraction leaking out at the back (b), as a function of the effective depth $< z >$ of the shower inside the calorimeter (top horizontal axis). The value of $< z >$ was determined from the displacement of the shower's lateral center of gravity with respect to the impact point of the pion ($\Delta x$, bottom horizontal axis). Data for 150 GeV data at $\theta_z = 3^0$.

13. The energy spectrum measured in the leakage calorimeter for 80 GeV $\pi^-$ at $\theta_z = 2^0$ (a). The energy spectrum measured in the leakage calorimeter for 20 GeV muons that have traversed the SPACAL calorimeter (b).

14. Characteristic energy deposit profile for a muon traversing the leakage calorimeter. The signals in the individual towers are given in units of 1/4 GeV.

15. Characteristic energy deposit profiles in the leakage calorimeter for charged hadrons escaping from the main calorimeter and strongly interacting in the leakage detector. The signals in the individual towers are given in units of 1/4 GeV.

16. Characteristic energy deposit profiles for neutrons escaping from the main calorimeter and interacting somewhere in the leakage detector. The signals in the individual towers are given in units of 1/4 GeV.

17. Energy deposit profiles in the SPACAL calorimeter (only the central part is shown) and in the leakage calorimeter. Typical examples of a pion shower in which a muon is produced (a) and of a muon from the beam contamination (b). The signals in the individual towers are given in units of 1/4 GeV. Data taken at 40 GeV.

18. The probability that an escaping muon is created in the hadronic shower development in the SPACAL detector, as a function of the energy of the incoming pion.

19. Signal distributions in the SPACAL detector for contained pion showers (a) and for pion showers in which a muon is generated (b). Data taken at 80 GeV and at $\theta_z = 2^0$.

20. The rates of soft neutrons and hadrons escaping the $9.5\lambda_I$ deep calorimeter, as a function of the energy of the incoming pion. The rates are normalized to the rate for muon production (see fig. 18, Table 3). No acceptance corrections were made. The curves are drawn to guide the eye.

# TABLE CAPTIONS

1. Hadronic shower leakage from a $9.5\lambda_I$ deep lead/scintillating-fiber calorimeter, for different energies. Listed are the pion energy, the number of pion showers, the fraction of these events that have less than 25 MeV longitudinal leakage, the average longitudinal leakage energy per event, the acceptance of the leakage calorimeter, the acceptance corrected average leakage energy per event and the average fraction of the pion energy that escapes from the back of the detector. Data for $\theta_z = 0^0$ (a) and $\theta_z = 3^0$ (b).

2. Hadronic shower leakage from a $9.5\lambda_I$ deep lead/scintillating-fiber calorimeter, for pions entering the detector at different angles (see text). Data for 40 GeV $\pi^-$. Listed are the pion energy, the number of pion showers, the fraction of these events that have less than 25 MeV longitudinal leakage, the average longitudinal leakage energy per event, the acceptance of the leakage calorimeter, the acceptance-corrected average leakage energy per event and the average fraction of the pion energy that escapes from the back of the detector.

3. Muon production in hadronic shower development in a $9.5\lambda_I$ deep lead/ scintillating-fiber calorimeter. Listed are the pion energy, the number of pion showers, the number of events in which a muon is produced in the shower development, the acceptance of the detector with which these muons were measured, the acceptance-corrected number of events in which a muon is produced, the fraction of the pion showers in which a muon is generated and the difference between the average signals from events without and with a muon. Data for $\theta_z = 0^0$.

4. The relative rates of muons, hadrons and neutrons measured in the leakage calorimeter. Listed are for each shower energy the number of pion showers, the measured numbers of escaping muons, hadrons and neutrons, and the hadron and neutron rates relative to the muon one. The data are not corrected for acceptance and the errors are statistical only. Data for $\theta_z = 0^0$.

| Table 1a ($\theta_z = 0^0$) | | | | | | |
|---|---|---|---|---|---|---|
| $E_\pi$ (GeV) | events | % contained | $\bar{E}_{LC}$ (GeV) | acceptance | $\bar{E}_{LC}^{corr}$ (GeV) | leakage (%) |
| 5 | 300 | - | - | - | - | - |
| 10 | 2648 | 97.2 | 0.003±0.001 | 0.75 ×0.74 | 0.006±0.002 | 0.06±0.02 |
| 20 | 2352 | 90.8 | 0.011±0.002 | 0.75 ×0.74 | 0.020±0.004 | 0.11±0.01 |
| 40 | 2805 | 89.2 | 0.047±0.007 | 0.75 ×0.74 | 0.085±0.013 | 0.22±0.02 |
| 80 | 3272 | 84.9 | 0.143±0.018 | 0.75 ×0.74 | 0.260±0.033 | 0.33±0.02 |
| 150 | 3255 | 74.7 | 0.347±0.029 | 0.75 ×0.74 | 0.631±0.053 | 0.42±0.02 |

| Table 1b ($\theta_z = 3^0$) | | | | | | |
|---|---|---|---|---|---|---|
| $E_\pi$ (GeV) | events | % contained | $\bar{E}_{LC}$ (GeV) | acceptance | $\bar{E}_{LC}^{corr}$ (GeV) | leakage (%) |
| 5 | 300 | - | - | - | - | - |
| 10 | 2506 | 98.1 | 0.002±0.001 | 0.75 ×0.74 | 0.004±0.001 | 0.04±0.01 |
| 20 | 2260 | 91.6 | 0.009±0.002 | 0.75 ×0.74 | 0.016±0.004 | 0.09±0.01 |
| 40 | 2781 | 90.2 | 0.037±0.005 | 0.75 ×0.74 | 0.067±0.009 | 0.18±0.02 |
| 80 | 3168 | 87.0 | 0.097±0.012 | 0.75 ×0.74 | 0.176±0.022 | 0.23±0.02 |
| 150 | 3227 | 75.4 | 0.330±0.029 | 0.75 ×0.74 | 0.600±0.053 | 0.40±0.02 |

| Table 2 (40 GeV $\pi^-$) | | | | | | |
|---|---|---|---|---|---|---|
| $\theta_z(^0)$ | events | % contained | $\bar{E}_{LC}$ (GeV) | acceptance | $\bar{E}_{LC}^{corr}$ (GeV) | leakage (%) |
| 0 | 2805 | 89.2 | 0.047±0.007 | 0.75 ×0.74 | 0.085±0.013 | 0.22±0.02 |
| 1 | 2776 | 90.8 | 0.069±0.012 | 0.75 ×0.74 | 0.125±0.022 | 0.33±0.02 |
| 2 | 2797 | 91.3 | 0.029±0.004 | 0.75 ×0.74 | 0.052±0.007 | 0.14±0.02 |
| 3 | 2781 | 90.2 | 0.037±0.005 | 0.75 ×0.74 | 0.067±0.009 | 0.18±0.02 |
| 4 | 2843 | 89.4 | 0.040±0.006 | 0.75 ×0.74 | 0.073±0.011 | 0.19±0.02 |
| 5 | 5657 | 90.2 | 0.033±0.004 | 0.75 ×0.74 | 0.060±0.007 | 0.16±0.02 |

| Table 3 | | | | | | |
|---|---|---|---|---|---|---|
| $E_\pi$ (GeV) | events | muons | acceptance | muons (corr.) | $\mu$-rate (%) | $E_{miss}$ (GeV) |
| 10 | 2751 | 4±2.2 | 0.75 | 5.3±3.0 | 0.19±0.11 | 1.4±0.9 |
| 20 | 2352 | 5±2.4 | 0.75 | 6.7±3.3 | 0.28±0.14 | 2.9±2.9 |
| 40 | 2805 | 10±3.7 | 0.75 | 13.4±5.0 | 0.48±0.18 | 2.6±1.1 |
| 80 | 3272 | 30±8.1 | 0.75 | 40.0±11.0 | 1.22±0.34 | 4.6±1.5 |
| 150 | 3255 | 51±8.7 | 0.75 | 68.1±12.2 | 2.09±0.37 | 4.6±1.8 |

| Table 4 | | | | | | |
|---|---|---|---|---|---|---|
| $E_\pi$ (GeV) | events | muons | hadrons | neutrons | hadron/$\mu$ | neutron/$\mu$ |
| 20 | 2352 | 5 | 6 | 181 | 1.2±0.7 | 36±16 |
| 40 | 2805 | 10 | 18 | 211 | 1.8±0.7 | 21±7 |
| 80 | 3272 | 30 | 121 | 299 | 4.0±0.8 | 10.0±1.9 |
| 150 | 3255 | 51 | 304 | 442 | 6.0±0.9 | 8.7±1.2 |

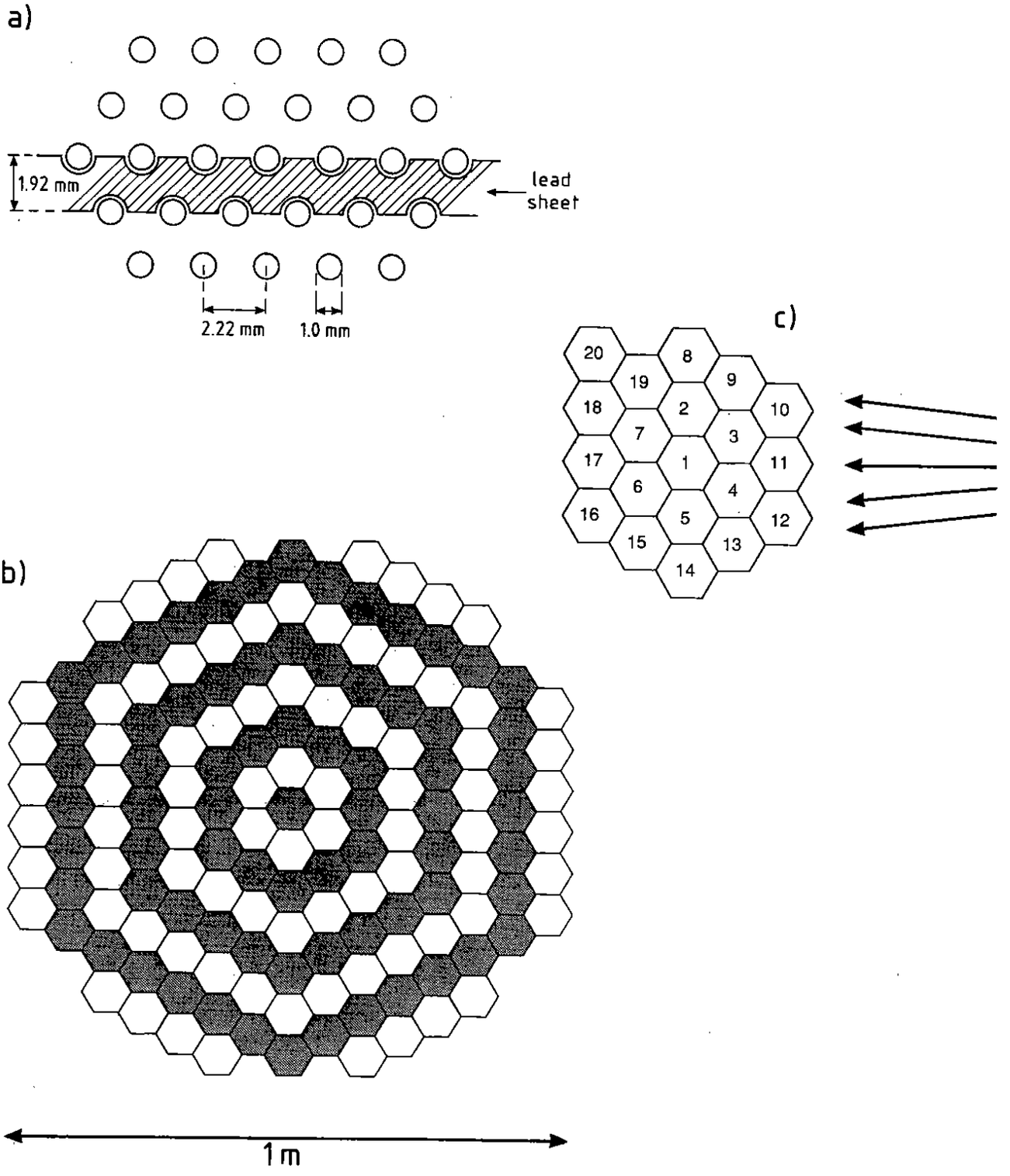
a)
1.92 mm
lead sheet
2.22 mm
1.0 mm
c)
20
8
19
9
18
2
10
7
3
17
1
11
6
4
16
5
12
15
13
14
b)
1 m

Figure 1

Figure 2

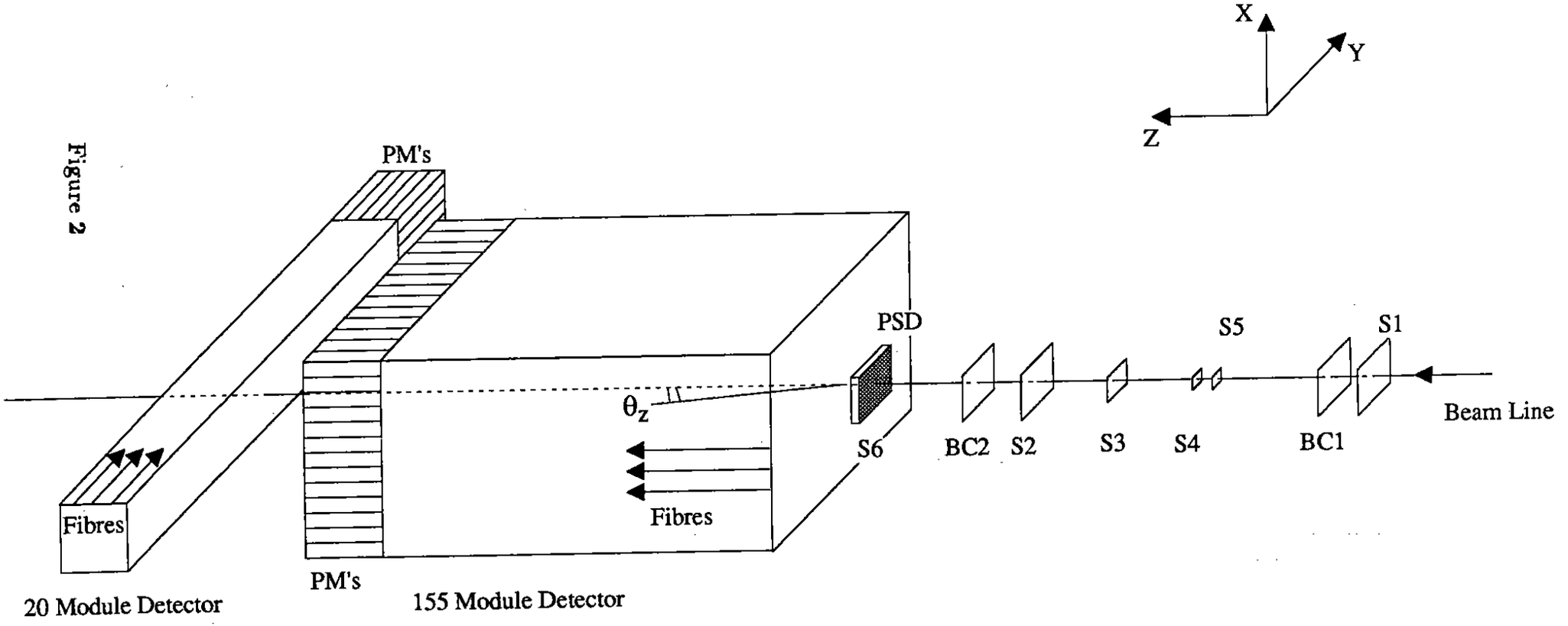


Not to scale

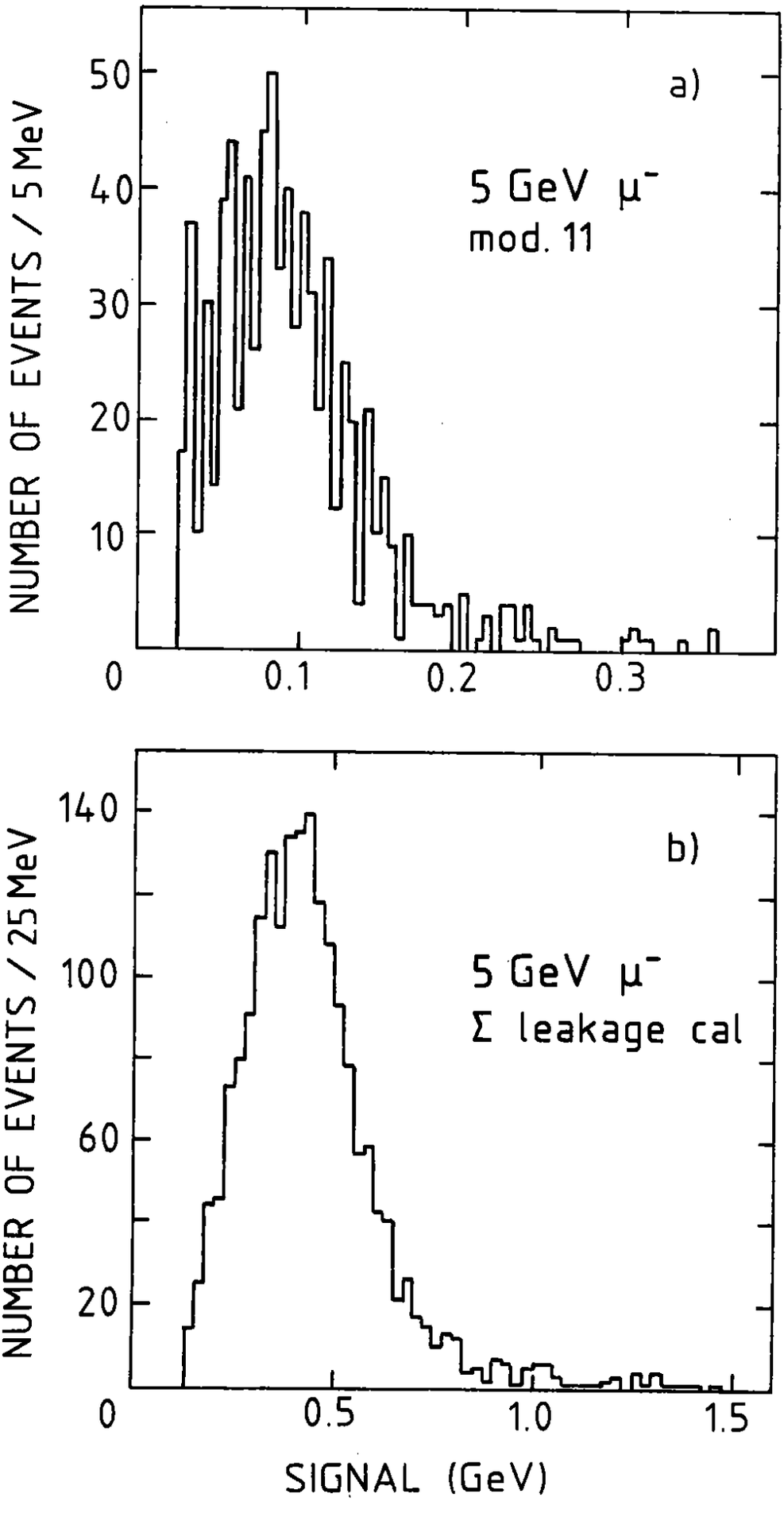
a)
5 GeV μ⁻
mod. 11
NUMBER OF EVENTS / 5 MeV
50
40
30
20
10
0
0.1
0.2
0.3
b)
5 GeV μ⁻
Σ leakage cal
NUMBER OF EVENTS / 25 MeV
140
100
60
20
0
0.5
1.0
1.5
SIGNAL (GeV)

**Figure 3**

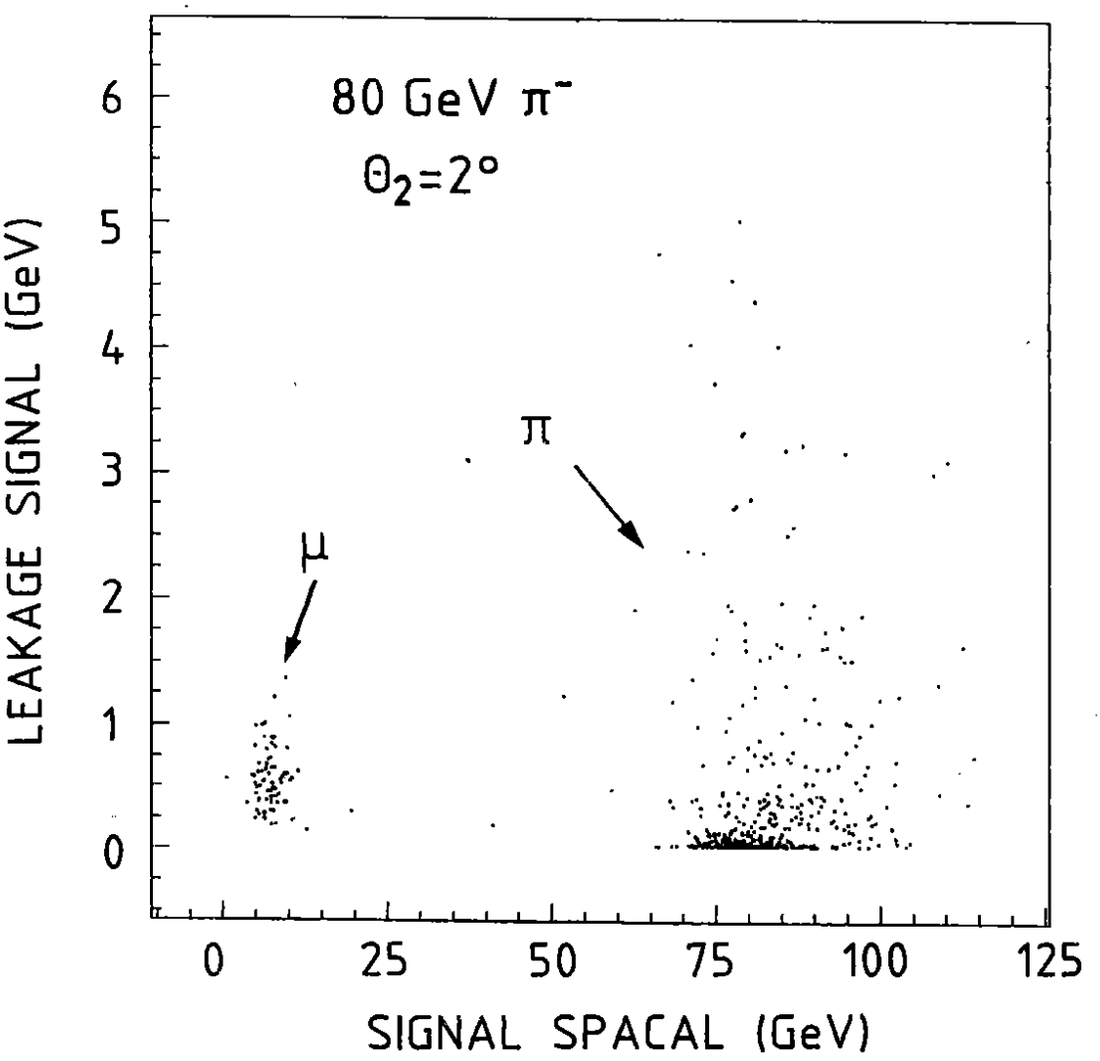
80 GeV π⁻
θ2=2°
π
μ
LEAKAGE SIGNAL (GeV)
SIGNAL SPACAL (GeV)
0
1
2
3
4
5
6
0
25
50
75
100
125

**Figure 4**

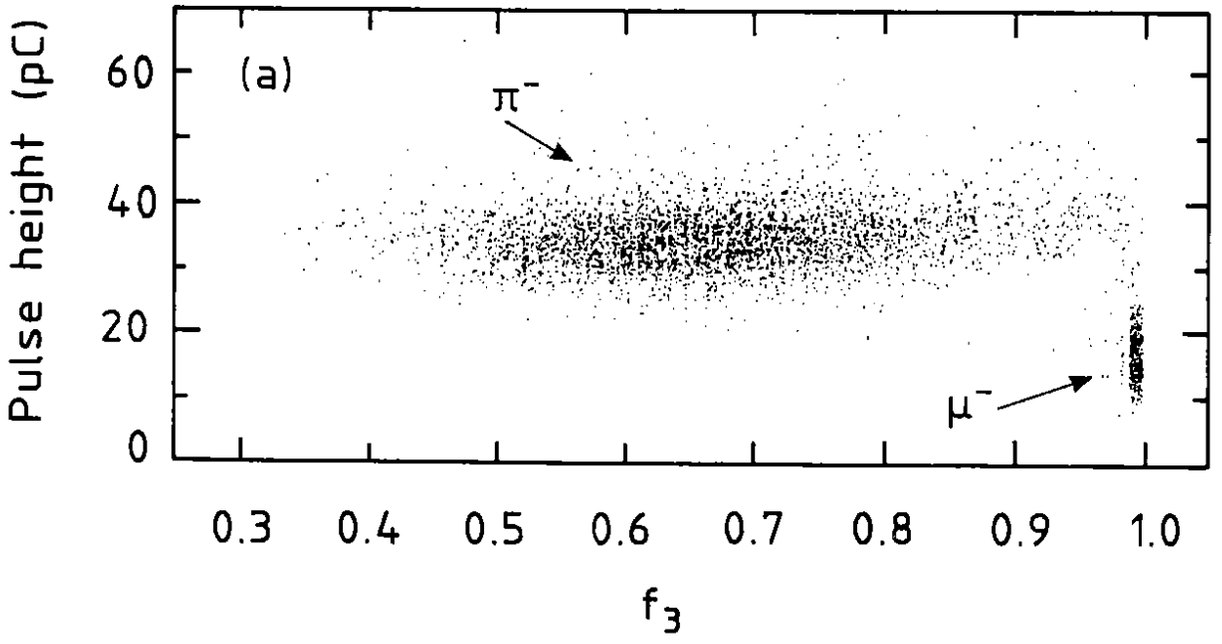


Figure 5

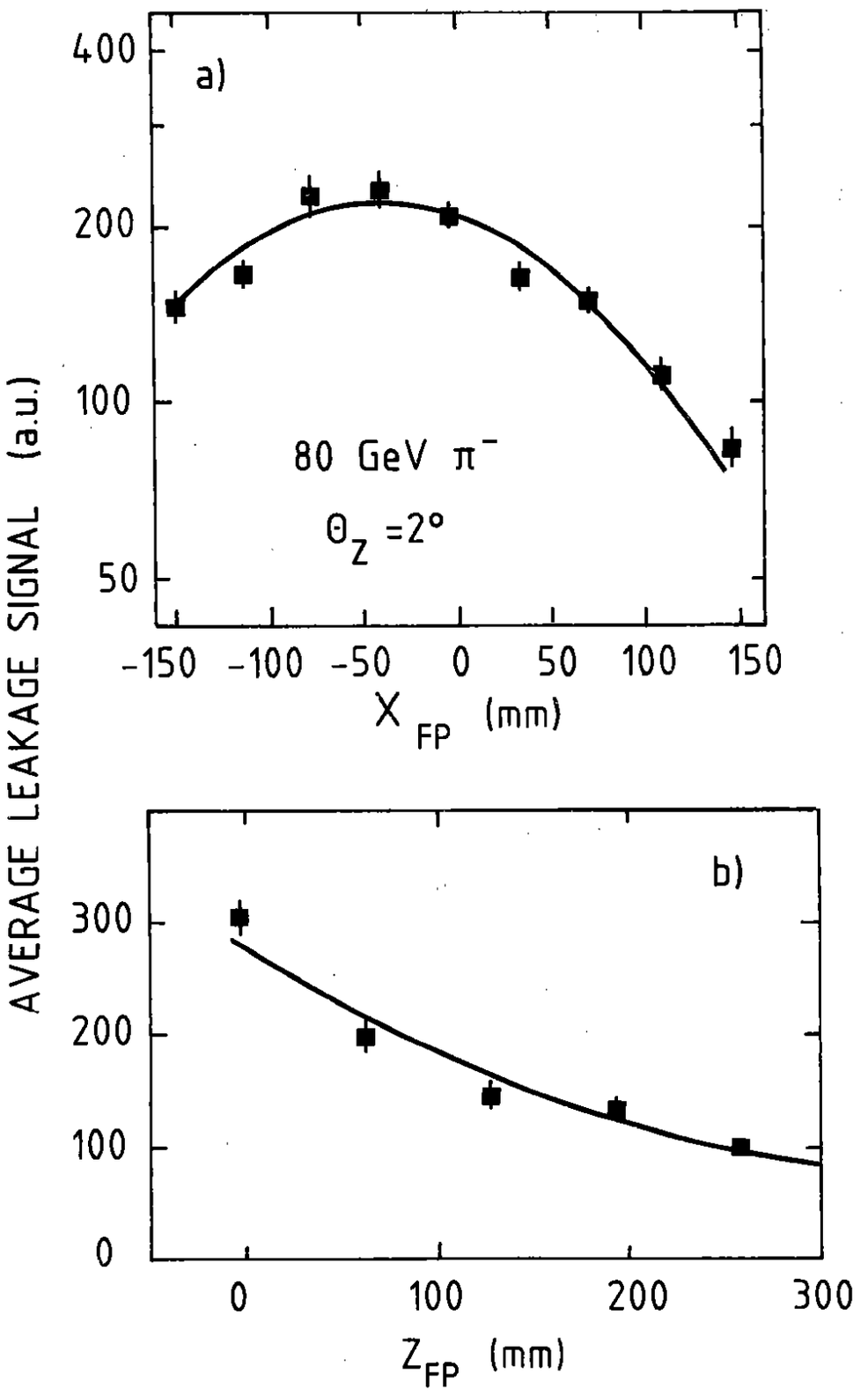
a)
400
200
100
50
80 GeV π⁻
θz =2°
-150 -100 -50 0 50 100 150
X FP (mm)
AVERAGE LEAKAGE SIGNAL (a.u.)
b)
300
200
100
0
0 100 200 300
Z FP (mm)

Figure 6

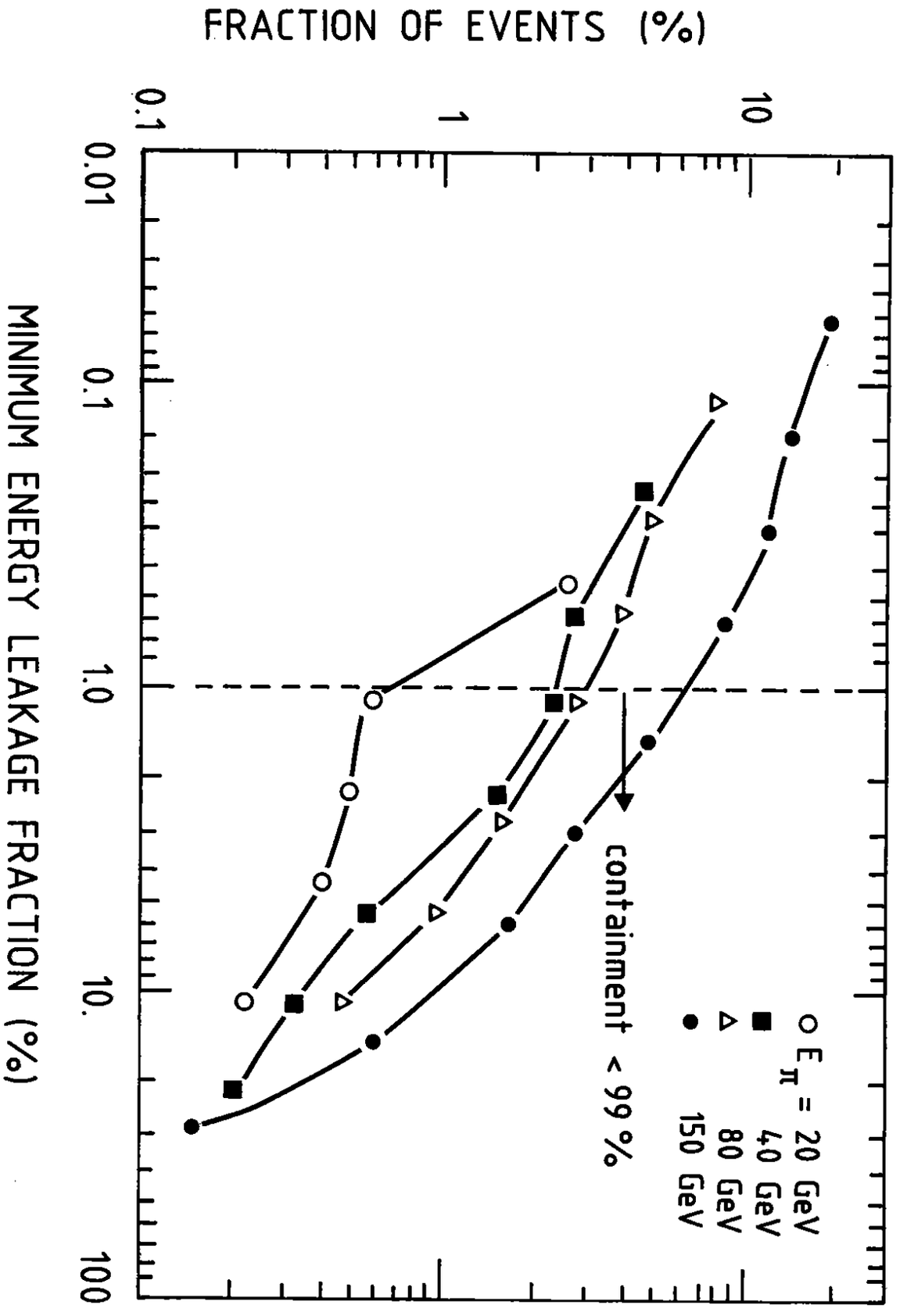
FRACTION OF EVENTS (%)
0.1
1
10
MINIMUM ENERGY LEAKAGE FRACTION (%)
0.01
0.1
1.0
10.
100
containment < 99 %
E_π = 20 GeV
40 GeV
80 GeV
150 GeV

Figure 7

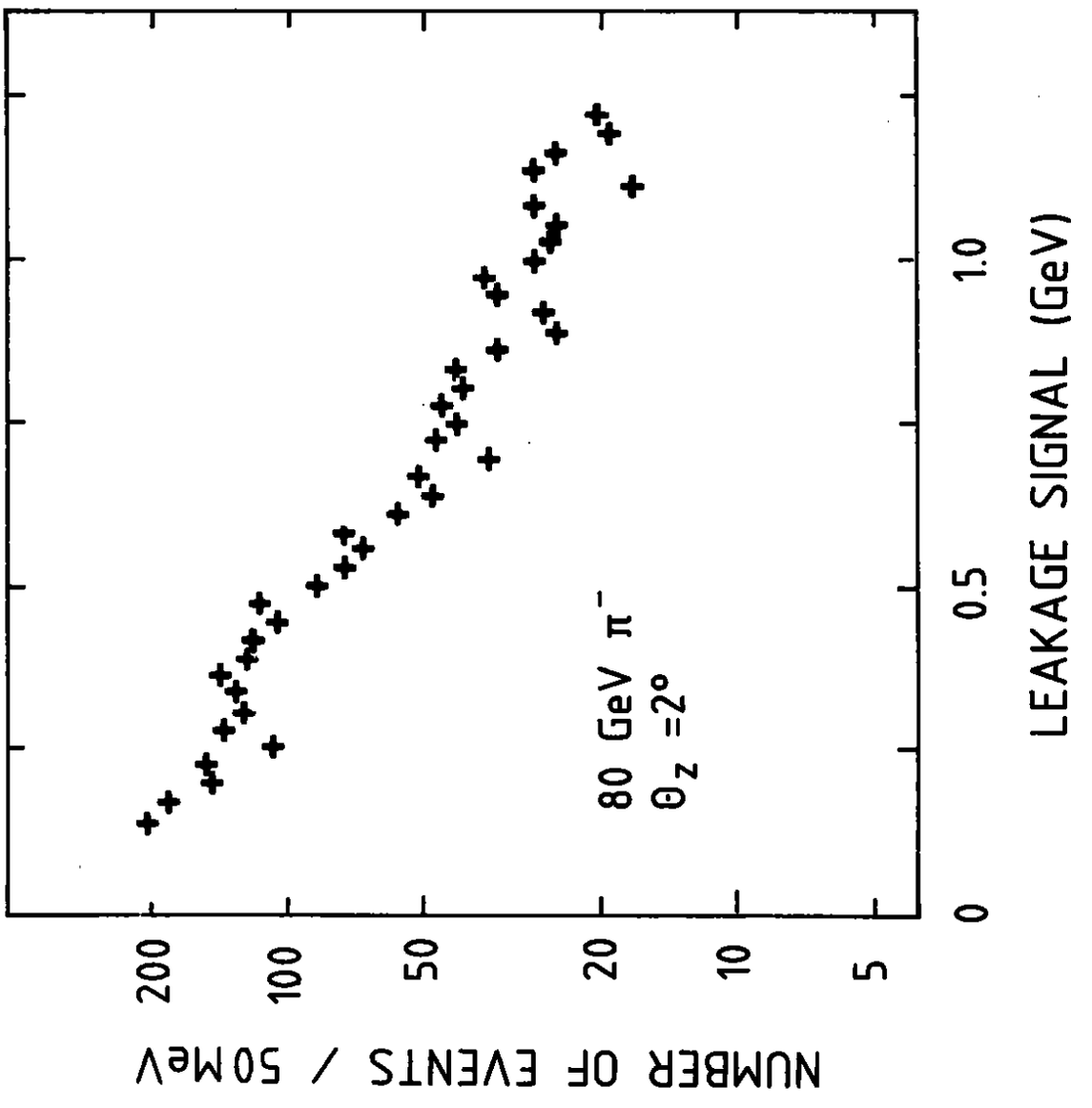
NUMBER OF EVENTS / 50MeV
200
100
50
20
10
5
0
0.5
1.0
LEAKAGE SIGNAL (GeV)
80 GeV π⁻
θz =2°

Figure 8

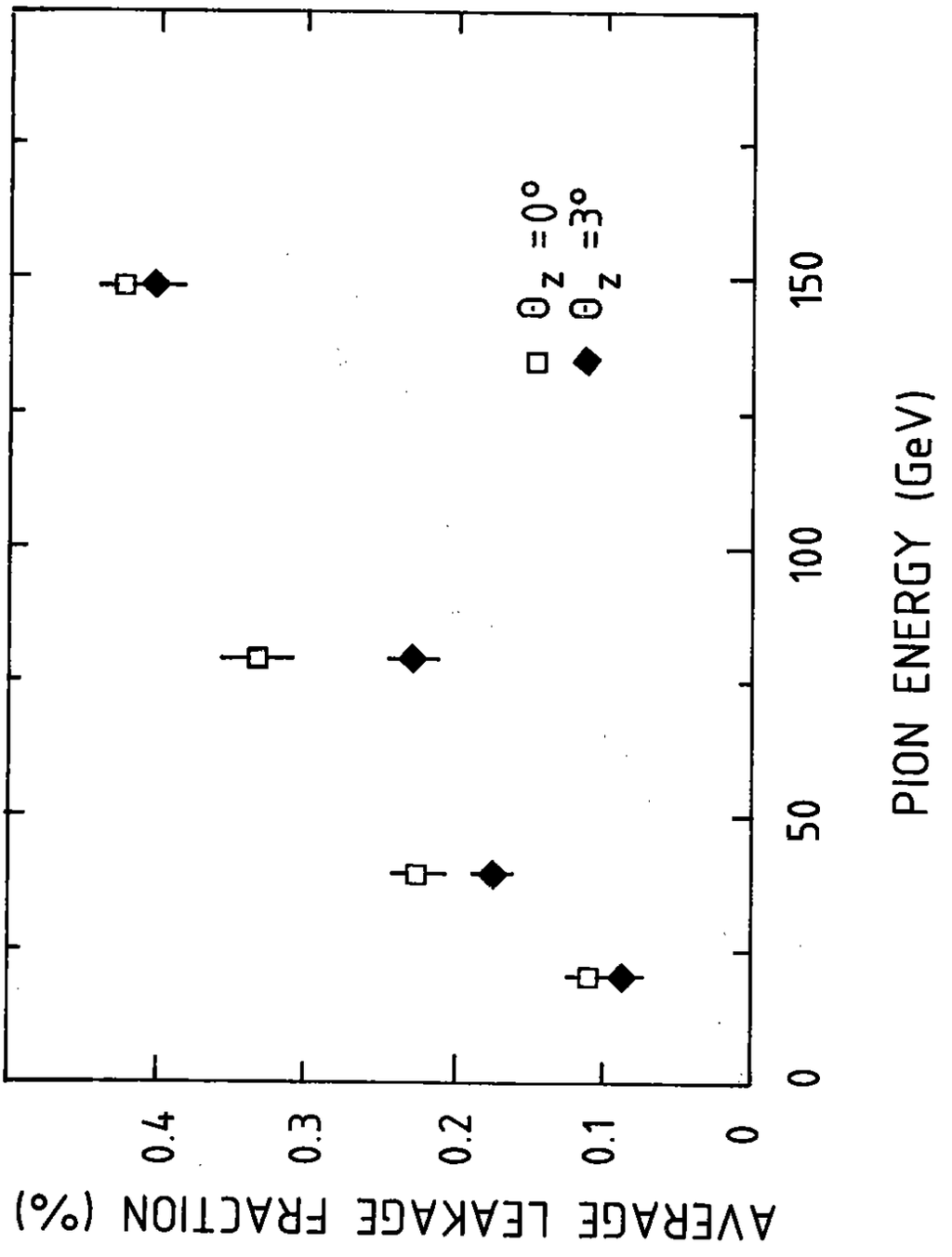
AVERAGE LEAKAGE FRACTION (%)
0.4
0.3
0.2
0.1
0
0
50
100
150
PION ENERGY (GeV)
θz =0°
θz =3°

Figure 9

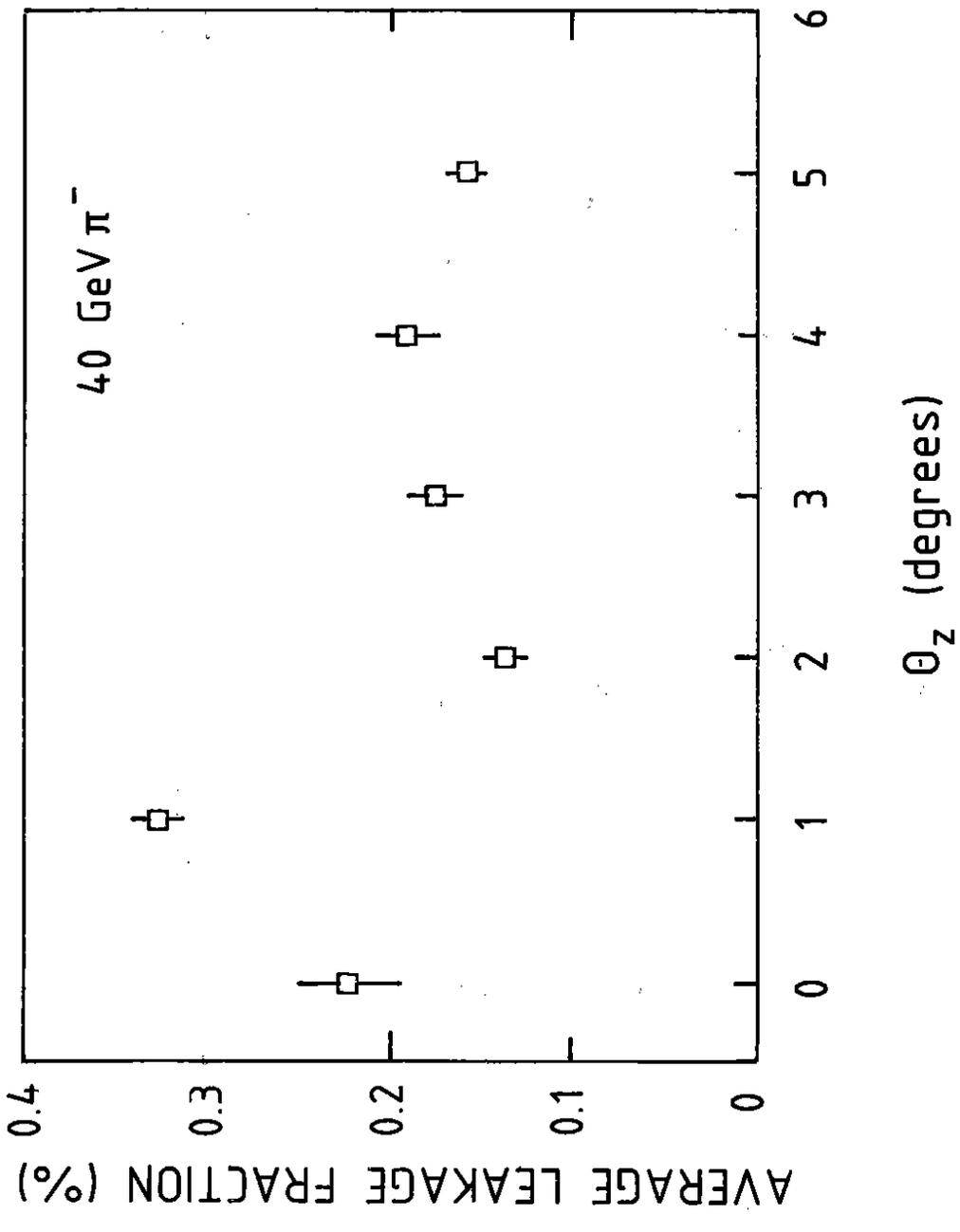
AVERAGE LEAKAGE FRACTION (%)
0.4
0.3
0.2
0.1
0
40 GeV π⁻
0
1
2
3
4
5
6
θz (degrees)

Figure 10

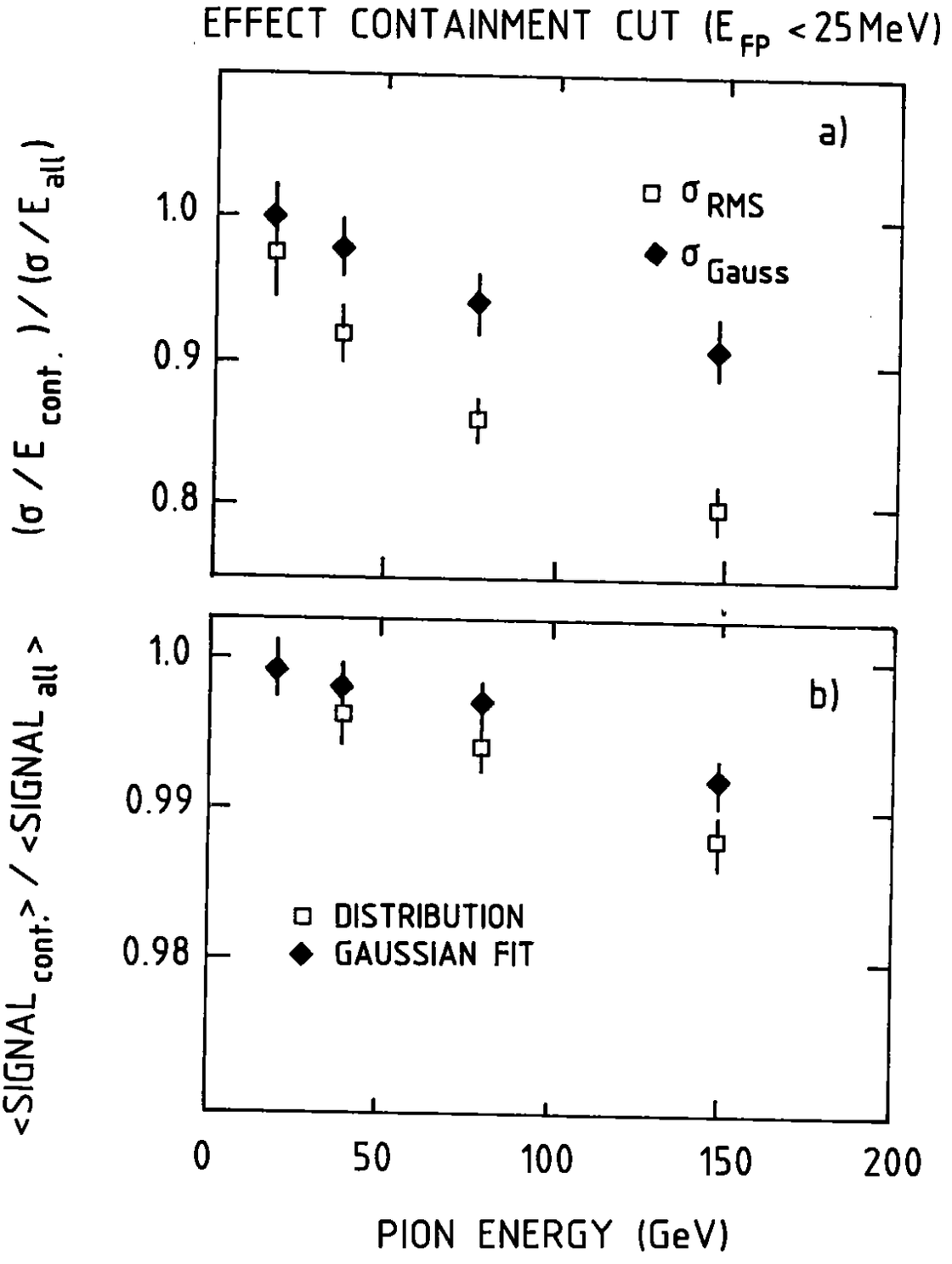
EFFECT CONTAINMENT CUT ($E_{FP}$ < 25 MeV)
a)
$\sigma_{RMS}$
$\sigma_{Gauss}$
1.0
0.9
0.8
$(\sigma / E_{cont.}) / (\sigma / E_{all})$
b)
DISTRIBUTION
GAUSSIAN FIT
1.0
0.99
0.98
$\langle SIGNAL_{cont.} \rangle / \langle SIGNAL_{all} \rangle$
0
50
100
150
200
PION ENERGY (GeV)

**Figure 11**

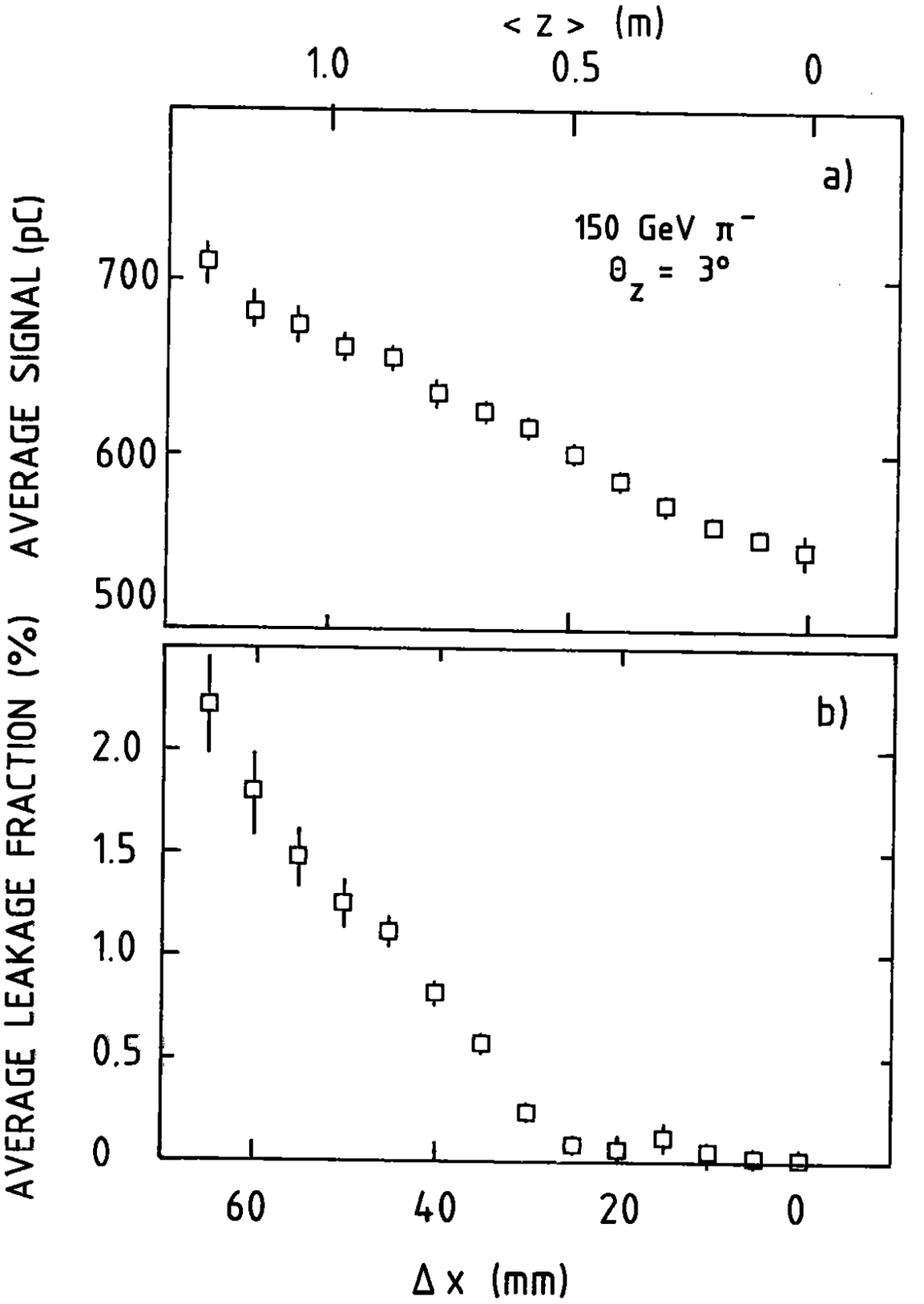
< z > (m)
1.0
0.5
0
a)
150 GeV π⁻
θz = 3°
700
600
500
b)
2.0
1.5
1.0
0.5
0
60
40
20
0
Δ x (mm)
AVERAGE LEAKAGE FRACTION (%) AVERAGE SIGNAL (pC)

Figure 12

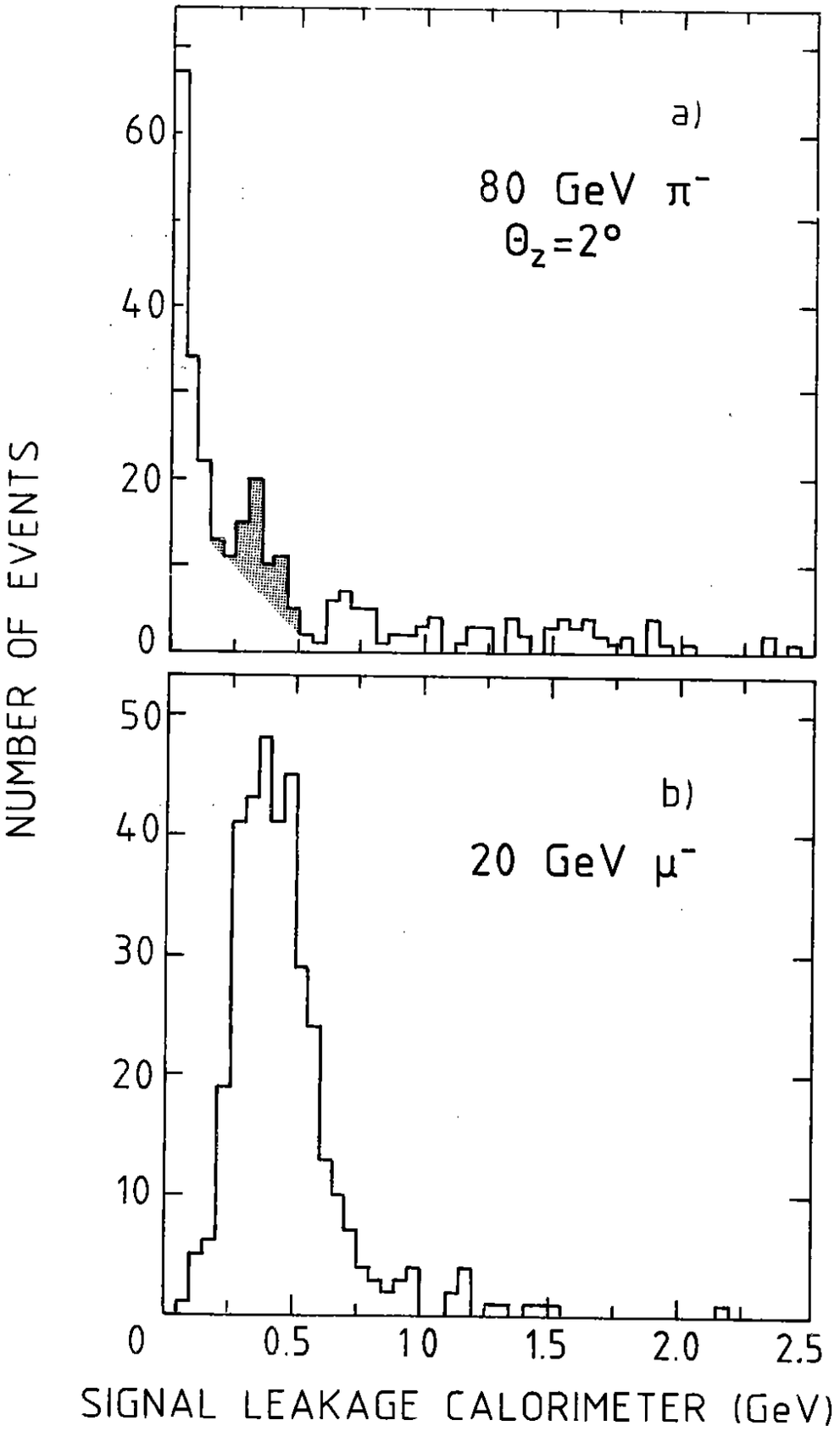
a)
80 GeV π⁻
θz=2°
b)
20 GeV μ⁻
NUMBER OF EVENTS
SIGNAL LEAKAGE CALORIMETER (GeV)
0
20
40
60
10
30
50
0.5
1.0
1.5
2.0
2.5

Figure 13

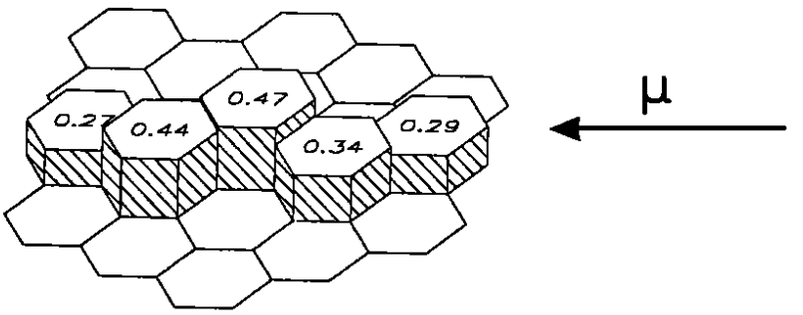


**Figure 14**

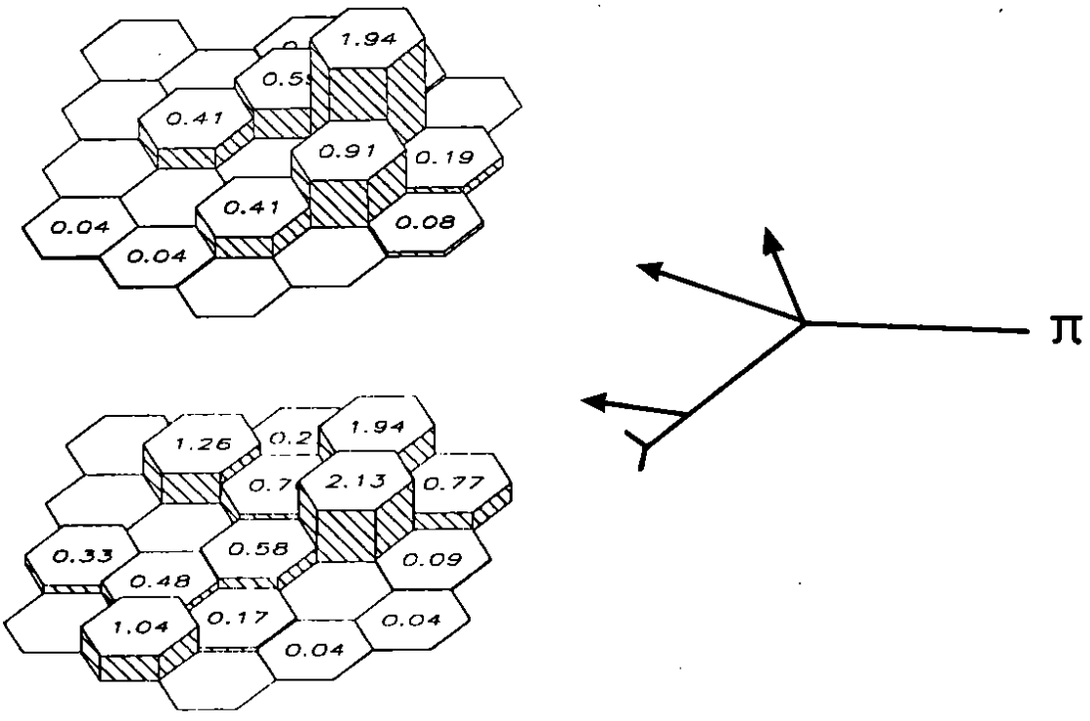
1.94
0.5
0.41
0.91
0.19
0.41
0.08
0.04
0.04
1.26
0.2
1.94
0.7
2.13
0.77
0.33
0.58
0.09
0.48
1.04
0.17
0.04
0.04
π

**Figure 15**

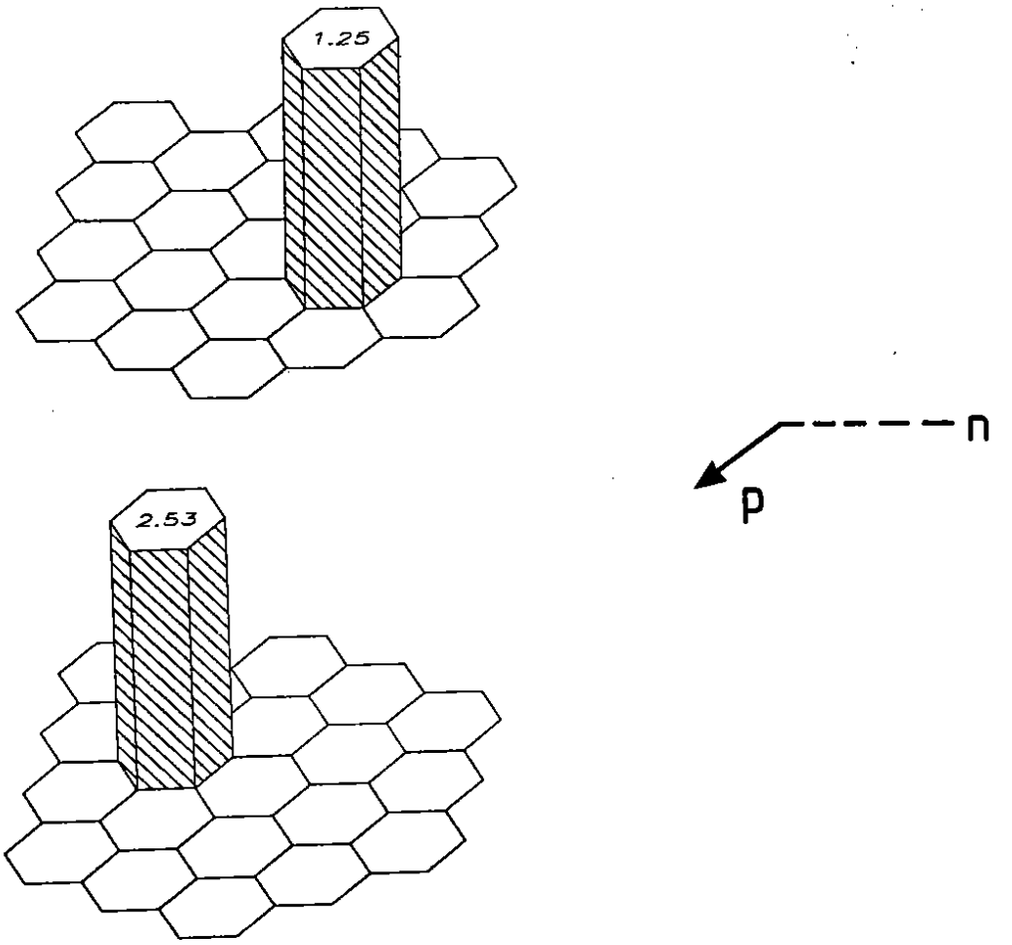


Figure 16

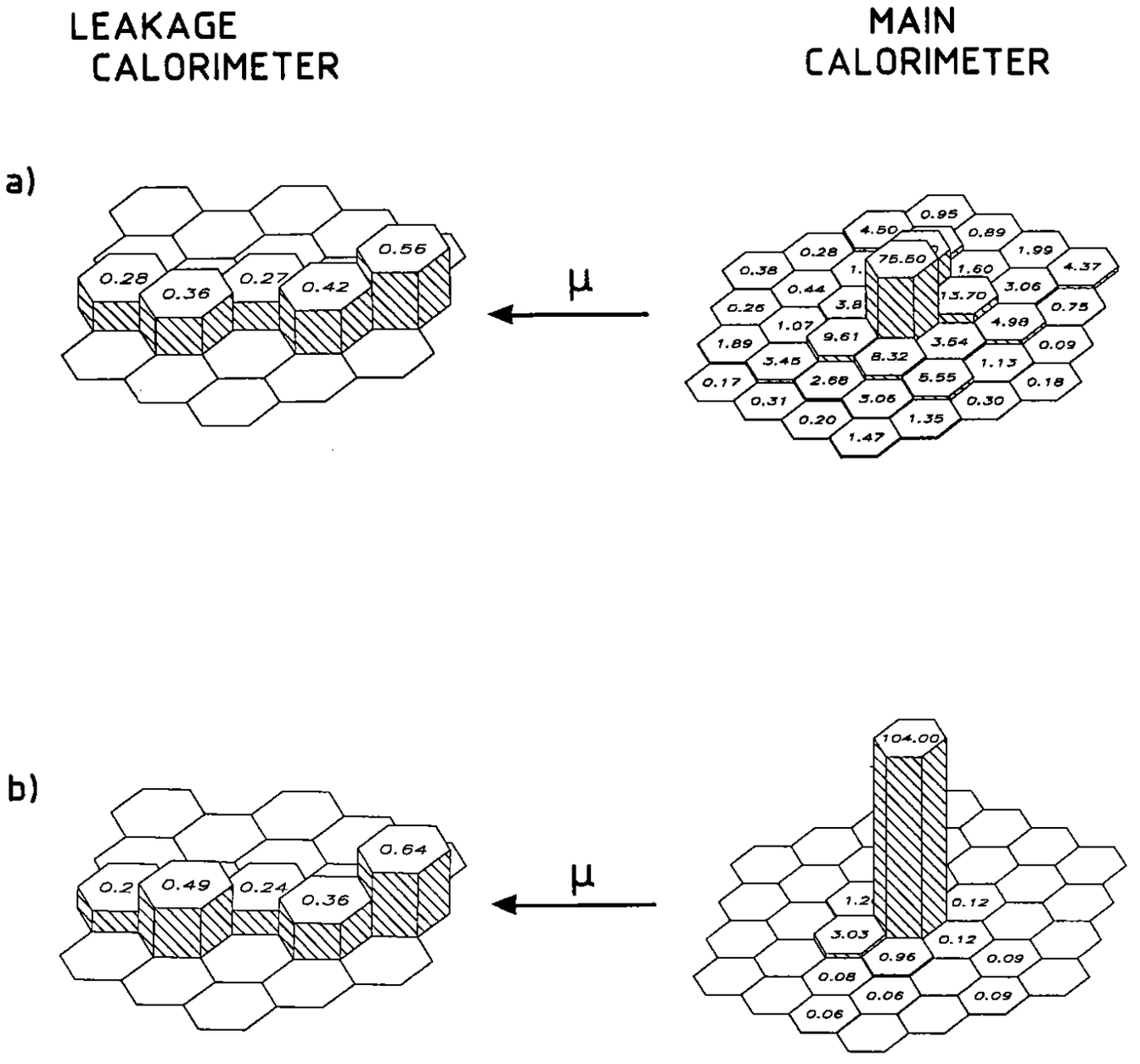
LEAKAGE
CALORIMETER
MAIN
CALORIMETER
a)
0.28
0.36
0.27
0.42
0.56
μ
0.95
4.50
0.89
0.28
1.99
0.38
1.
76.50
1.60
4.37
0.44
13.70
3.06
0.26
3.8
0.75
1.07
4.98
1.89
9.61
3.64
0.09
3.45
8.32
1.13
0.17
2.68
5.55
0.18
0.31
3.06
0.30
0.20
1.35
1.47
b)
0.2
0.49
0.24
0.36
0.64
μ
104.00
1.2
0.12
3.03
0.12
0.96
0.09
0.08
0.06
0.09
0.06

Figure 17

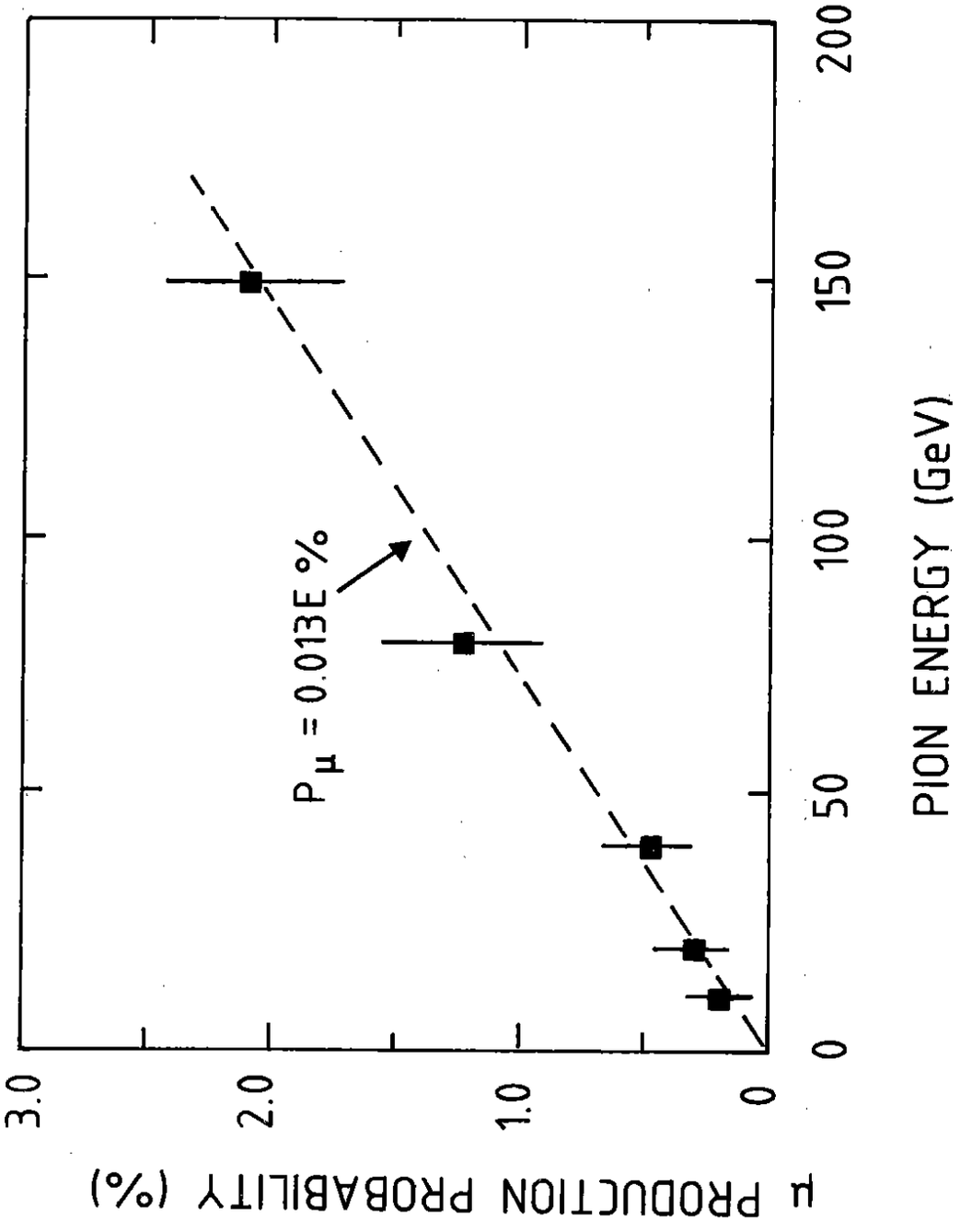
μ PRODUCTION PROBABILITY (%)
3.0
2.0
1.0
0
0
50
100
150
200
PION ENERGY (GeV)
$P_\mu = 0.013E$ %

Figure 18

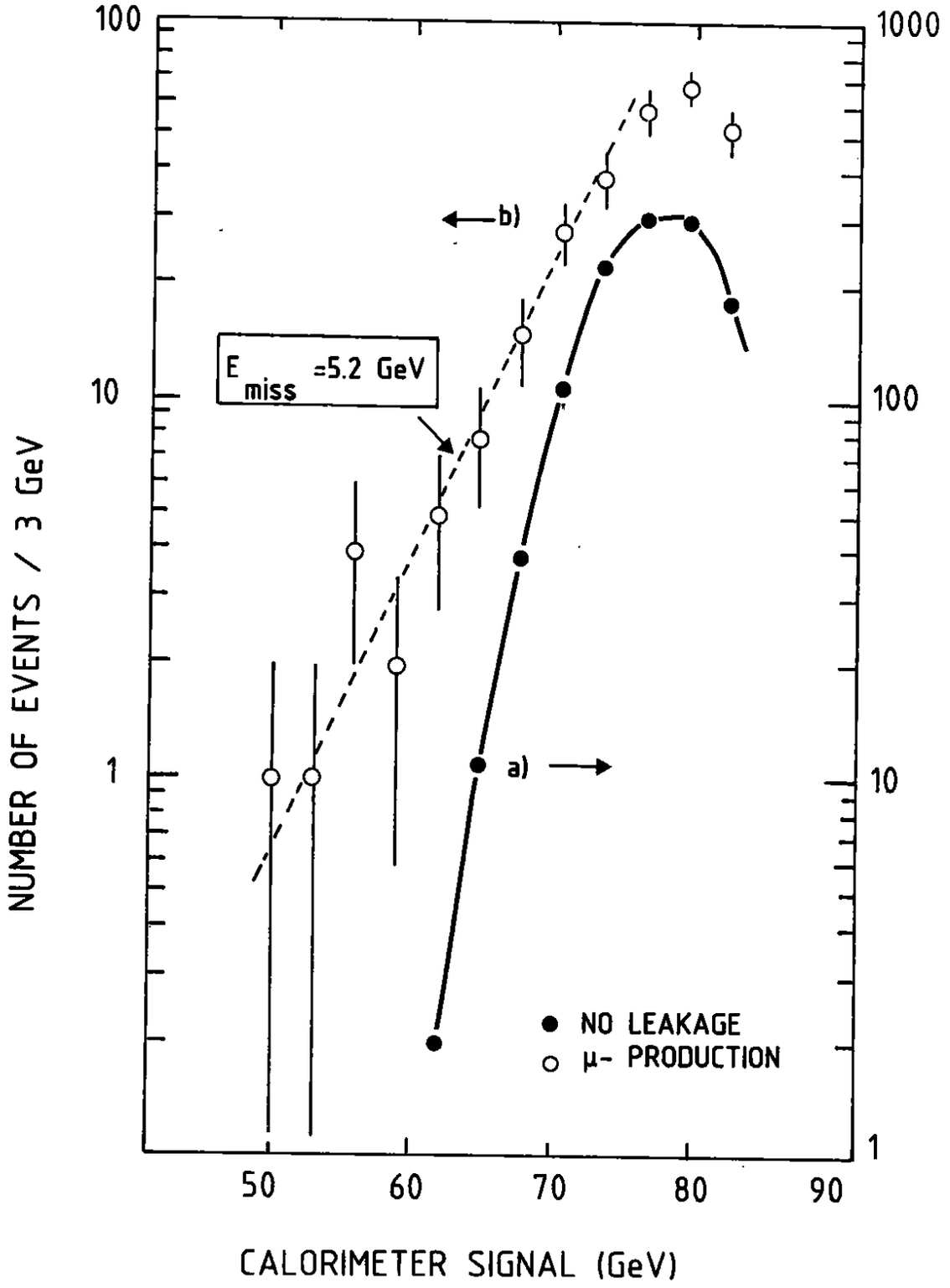
100
1000
10
100
1
10
1
b)
a)
E miss =5.2 GeV
NO LEAKAGE
μ- PRODUCTION
NUMBER OF EVENTS / 3 GeV
50
60
70
80
90
CALORIMETER SIGNAL (GeV)

Figure 19

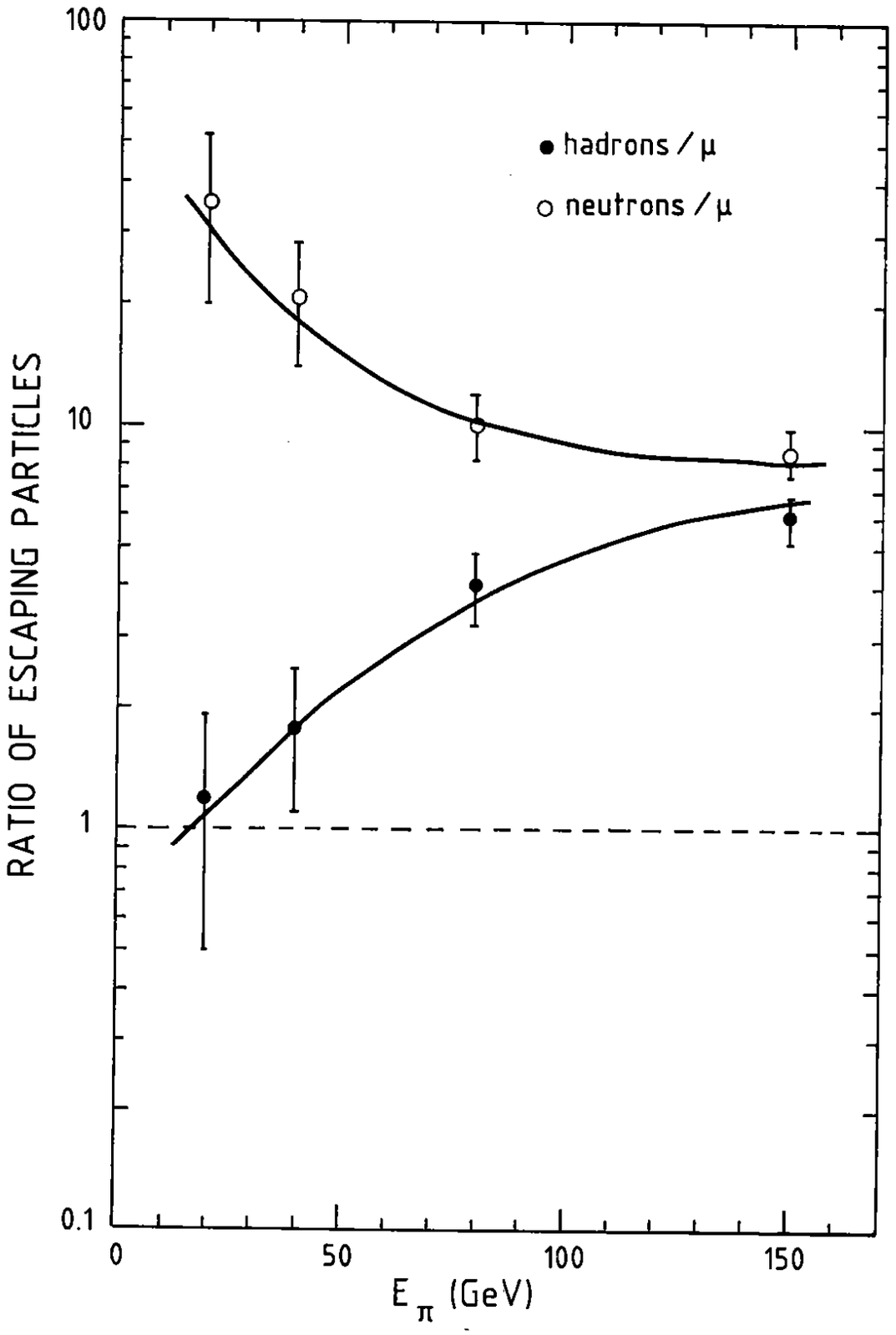


**Figure 20**

Imprimé au CERN. Prix : 1.40 Fr.